Electronic Supplementary Information (ESI)

New insights in the progressive ligand replacement from $[Ru_2Cl(O_2CCH_3)_4]$: synthetic strategies and variation of redox potentials and paramagnetic shifts

Almudena Inchausti,[a] Aarón Terán,[b] Alberto Manchado-Parra,[b] Alessandra de Marcos-Galán,[c‡] Josefina Perles,[c] Miguel Cortijo,[b] Rodrigo González-Prieto,[b] Santiago Herrero,[b,] and Reyes Jiménez-Aparicio[b*]*

[a] MALTA-Consolider Team and Departamento de Química Física, Facultad de Ciencias Químicas, Universidad Complutense de Madrid, E-28040 Madrid, Spain

[b] Departamento de Química Inorgánica, Facultad de Ciencias Químicas, Universidad Complutense de Madrid, E-28040 Madrid, Spain

[c] Laboratorio de difracción de Rayos X de Monocristal, Servicio Interdepartamental de Investigación, Universidad Autónoma de Madrid, E-28049 Madrid, Spain

[‡]Instituto de Tecnología Química, Universitat Politècnica de València – Consejo Superior de Investigaciones Científicas, E-46022, Valencia, Spain

*E-mail (R.J.-A.): reyesja@ucm.es

*E-mail (S.H.): sherrero@ucm.es

TABLE OF CONTENT

MATERIALS AND METHODS

$[Ru_2Cl(O_2CCH_3)_4]$ and *N,N'*-bis(4-fluorophenyl)formamidine (HD*p*-FPhF) were prepared following similar procedures to the ones described in the literature.[1,2] The reactants and solvents used in all the synthetic procedures described in this paper were obtained from commercial sources and used as received. Elemental analyses were carried out by the Microanalytical Service of the Complutense University of Madrid. Electrospray ionization (ESI) mass spectra were collected using an ion trap analyser HCT Ultra (Bruker Daltonics) mass spectrometer, and MALDI-TOF measurements were performed using an Ultraflex workstation (Bruker Daltonics), both in the Mass Spectrometry Service of the Complutense University of Madrid. FT-IR measurements were done with a PerkinElmer Spectrum 100 instrument with a universal ATR accessory. Magnetization measurements at variable temperature were performed in the Physical Techniques Service of the Complutense University of Madrid, using a Quantum Design MPMSXL SQUID magnetometer, correcting the diamagnetic contribution to the susceptibility of both the sample and its holder. Electronic spectra were measured in a Cary 5G spectrometer, in CH_2Cl_2 solutions with a concentration of ~10^{-4} M. Cyclic voltammograms were obtained using a Metrohm Autolab PGSTAT204 potentiostat, with a three-electrode system: glassy-carbon, a wire of Pt and Ag/AgCl as working, auxiliary and reference electrode, respectively. **1** – **4** solutions of 2 mg/mL concentration in tetrabutylammonium perchlorate (TBAP) 0.1 M solution in dichloromethane were nitrogen-degassed and measured at a scan rate of 0.1 V/s. The ferrocenium/ferrocene couple was observed at 0.52 V (vs. Ag/AgCl) in a TBAP 0.1 M solution in dichloromethane. ^{1}H and ^{19}F-NMR measurements were recorded at the NMR Service of the Complutense University of Madrid, using a Bruker AVIII spectrometer, operating at 300 MHz, and equipped with a BBOF 5mm ^{1}H / ^{19}F / BB probe. Chemical shifts were referenced to residual $CDHCl_2$(δ = 5.32 ppm) for ^{1}H spectra, while ^{19}F spectra were not referenced.

SINGLE-CRYSTAL X-RAY DIFFRACTION DATA COLLECTION AND STRUCTURE REFINEMENT

Single crystals of **1_n·$2CH_2Cl_2$**, **1DMSO·$2CH_2Cl_2$**, **$2H_2O$·$2H_2O$**, **3·$1.75CH_2Cl_2$** and **4·$CHCl_3$** were obtained as described in the corresponding synthetic procedure for each compound. Additionally, in the course of the synthesis optimization for compounds **1** and **2**, a few crystals of $[Ru_2Cl(Dp\text{-}FPhF)(O_2CCH_3)_3(OCHNHC_6H_4F)]\cdot 0.25CH_2Cl_2\cdot H_2O$ $0.5CH_2Cl_2$, $(Et_3NH)[Ru_2Cl_2(Dp\text{-}FPhF)(O_2CCH_3)_3]\cdot 0.5CH_2Cl_2$, and $[Ru_2Cl(Dp\text{-}FPhF)_2(O_2CCH_3)_2(OCHNHC_6H_4F)]$ ($OCHNHC_6H_4F$ = *N*-(4-fluorophenyl)formamide) were obtained from the crude reaction mixtures. Single crystals of **1_n·$2CH_2Cl_2$** and **4·$CHCl_3$** were measured at 150 and 250 K, respectively, while **1DMSO·$2CH_2Cl_2$** and **3·$1.5CH_2Cl_2$** were measured at 200 K, and **$2H_2O$·$2H_2O$**, $[Ru_2Cl(Dp\text{-}FPhF)(O_2CCH_3)_3(OCHNHC_6H_4F)]\cdot 0.25CH_2Cl_2\cdot H_2O$, $(Et_3NH)[Ru_2Cl_2(Dp\text{-}FPhF)(O_2CCH_3)_3]\cdot 0.5CH_2Cl_2$, and $[Ru_2Cl(Dp\text{-}FPhF)_2(O_2CCH_3)_2(OCHNHC_6H_4F)]$ at 296 K. A Bruker Kappa Apex II system was used for data acquisition except for **$2H_2O$·$2H_2O$** and $[Ru_2Cl(Dp\text{-}FPhF)_2(O_2CCH_3)_2(OCHNHC_6H_4F)]$, that were measured using a Bruker Smart-CCD diffractometer. Both diffractometers use graphite−monochromated Mo Kα radiation (λ = 0.71073 Å) from conventional sealed tubes.

INFRARED SPECTROSCOPY

Vibrational spectra of compounds **1** – **4** are shown in Fig. S1. Fig. S2-S7 show individually the infrared spectra of the starting materials and compounds **1** – **4** between 3800 and 650 cm^{-1}.

Changes among ligand substitution have been monitored and marked in Fig. S1 as grey sections A – E. Firstly, in section A, a band centred around 1640 cm^{-1} is observed for compounds **1** and **2**, as well as a wide band in the 3400-3500 cm^{-1} range. This suggests the presence of water in these samples, in accordance with elemental analyses (see the experimental section). In mono- and bis-substituted Ru_2^{5+} compounds, the coordination of a neutral molecule, such as water or solvents, in the free axial position, is very common,[3–5] which could be causing the presence of these vibrational modes. Occasionally, a band centred around 1700 cm^{-1} appears in the spectra of compounds **1** and **2** (Fig. S8). This can be attributed to the presence of a secondary species containing *N*-(4-fluorophenyl)formamidine: $[Ru_2Cl(Dp\text{-}FPhF)(O_2CCH_3)_3(OCHNHC_6H_4F)]$ or $[Ru_2Cl(Dp\text{-}FPhF)_2(O_2CCH_3)_2(OCHNH\text{-}C_6H_4F)]$.

Acetate vibrational modes can be observed in grey zones C and E in Fig. S1, corresponding to COO stretching (around 1440 cm^{-1}) and bending (around 690 cm^{-1}), respectively. According to the literature, the difference between the asymmetric ($vCOO_a$) and symmetric ($vCOO_s$) stretches reflects the bonding of this ligand to the metal core.[6–8] In $[Ru_2Cl(O_2CCH_3)_4]$ (Fig. S2), there is a difference of approximately 80 cm^{-1} between them, indicating a bridging coordination consistent with previous experimental data.[6] In compounds **1** – **3**, this difference is maintained, and a decrease in their intensity as the replacement of acetate by formamidinate takes place can be highlighted, which also occurs for the carboxylate bending mode. In both cases, this decrease ends up in the disappearance of these normal modes of vibration in compound **4**, as expected, due to the absence of the acetate ligand.

Although the formamidinate vibrational structure analysis is challenging, due to the many bands present in the spectra, the identification of several normal modes of vibration can be useful to monitor the substitution reaction, as with the acetate modes. There are two vibrational modes related to the N-H bond that should be present only in

the infrared spectrum of HD*p*-FPhF (Fig. S3), specifically the stretching mode, around 3000 cm^{-}. The absence of this band in the infrared spectra of compounds **1** – **4** (Fig. S2-S7) supports the hydrogen loss for the formation of the ligand. Some of the formamidinate modes observed are indicated in the B (mixture of CN and CC aromatic stretches), and D (CH bending) grey zones in Fig. S1. Here, a sharpening of these vibrational bands, as well as an increase in intensity, from top to bottom, is noted, being most evident for the totally substituted complex **4**. This effect is opposite to the one observed in the carboxylate vibrational modes, as expected.

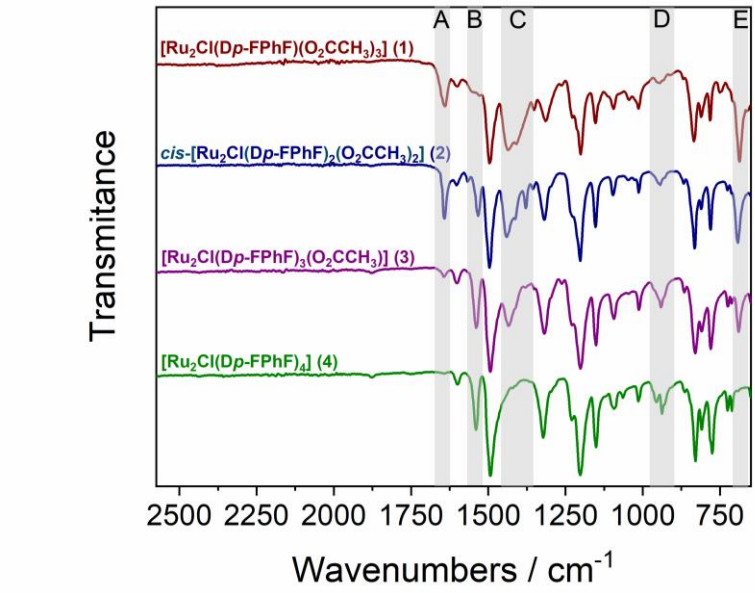

Fig. S1 Experimental infrared spectra of compounds, from top to bottom, **1** (wine red), **2** (navy blue), **3** (purple) and **4** (olive green), measured at room temperature. Grey zones represent HOH bending (A), a mixture of CN and CC aromatic stretches (B), carboxylate stretching (C), CH bending (D) and carboxylate bending (E) vibrational normal modes.

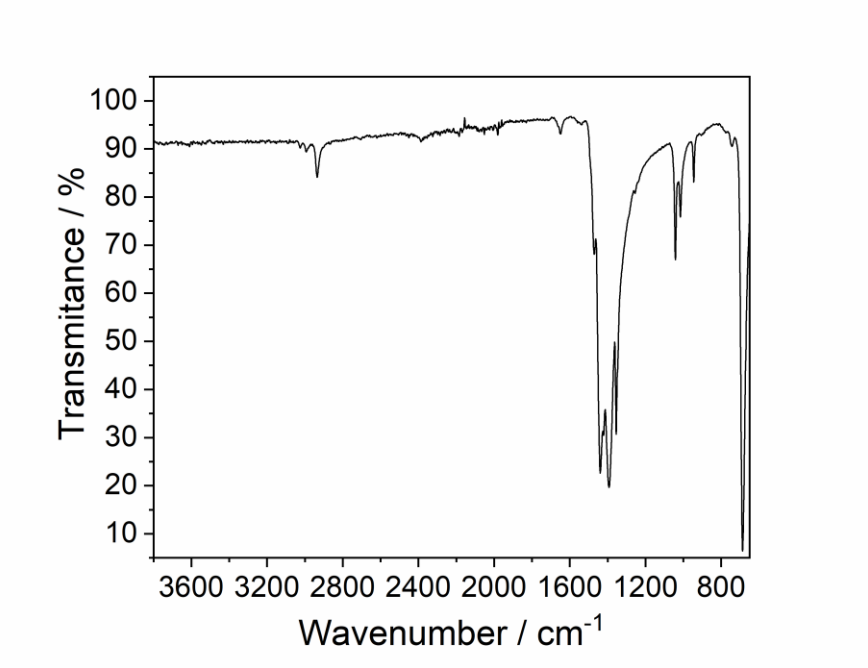

Fig. S2 Experimental infrared spectrum, in the range of 3800-650 cm^{-1}, of compound $[Ru_2Cl(O_2CCH_3)_4]$.

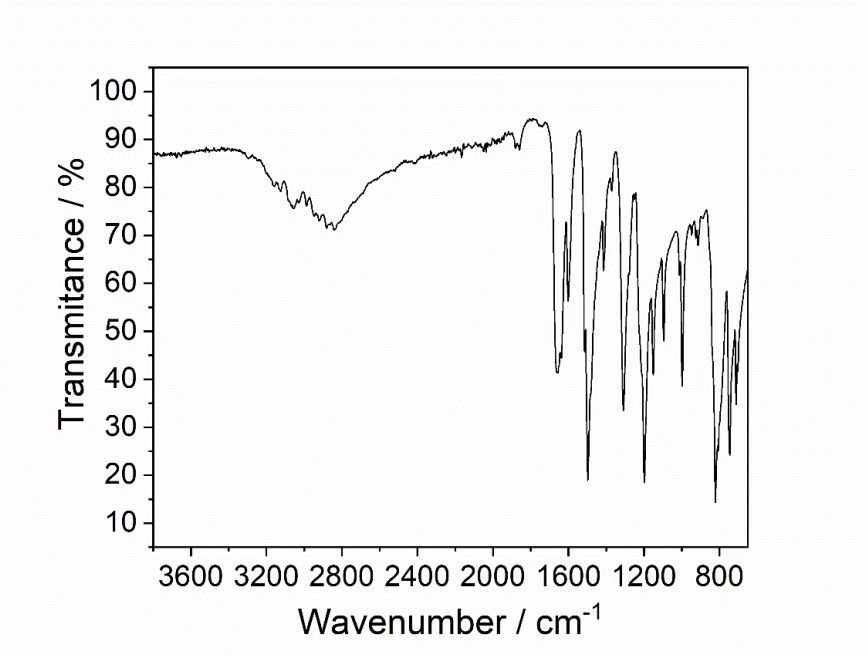

Fig. S3 Experimental infrared spectrum, in the range of 3800-650 cm^{-1}, of compound *N,N'*-bis(4-fluorophenyl)formamidine (HD*p*-FPhF).

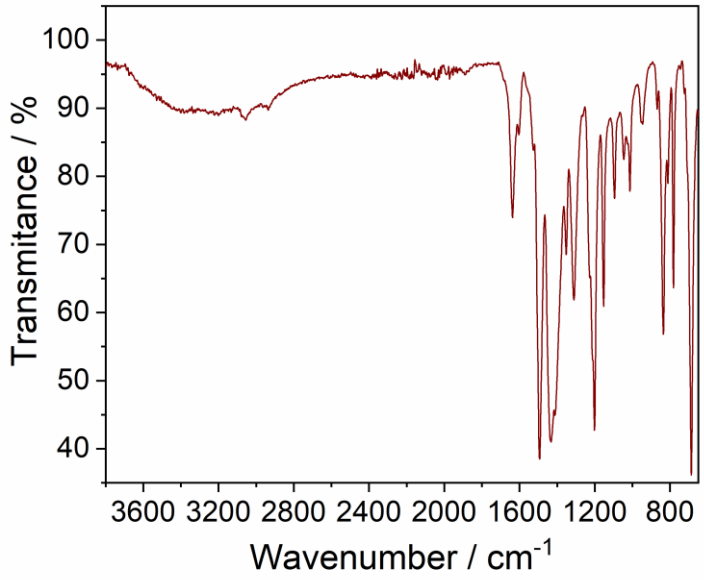

Fig. S4 Experimental infrared spectrum, in the range of 3800-650 cm^{-1}, of compound $[Ru_2Cl(D$*p*-$FPhF)(O_2CCH_3)_3(OH_2)]$ (**1H_2O**).

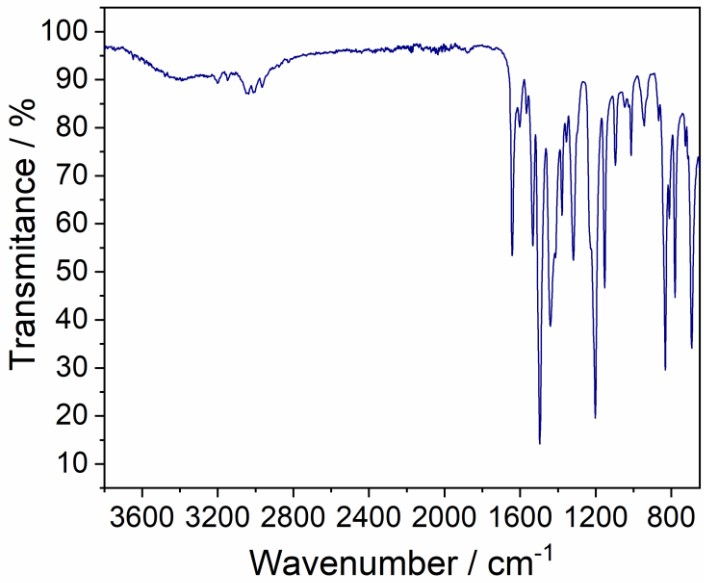

Fig. S5 Experimental infrared spectrum, in the range of 3800-650 cm^{-1}, of compound $[Ru_2Cl(D$*p*-$FPhF)_2(O_2CCH_3)_2(OH_2)]\cdot 0.5H_2O$ (**2H_2O·0.5H_2O**).

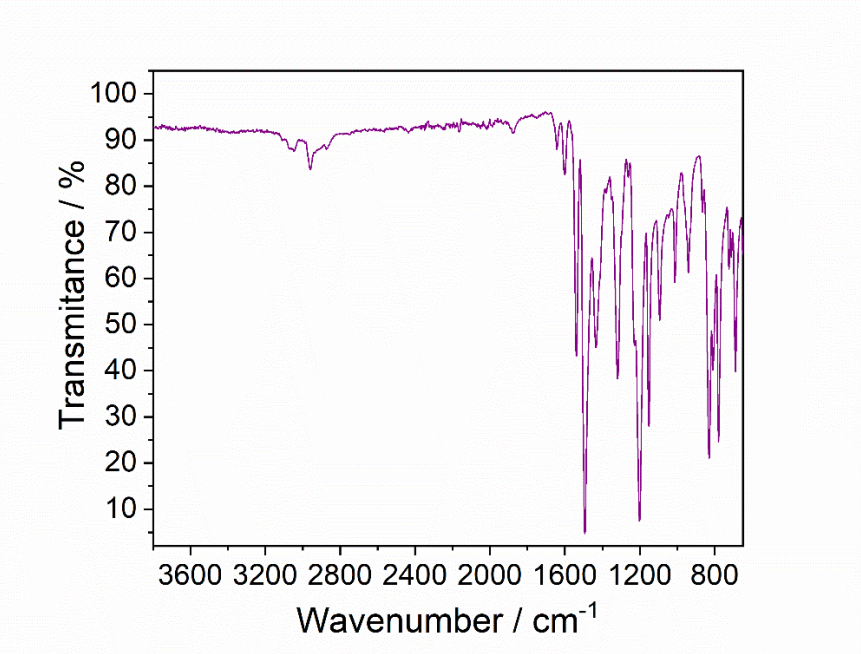

Fig. S6 Experimental infrared spectrum, in the range of 3800-650 cm^{-1}, of compound $[Ru_2Cl(D$*p*-$FPhF)_3(O_2CCH_3)]\cdot 0.5Et_2O$ (**3·0.5Et₂O**).

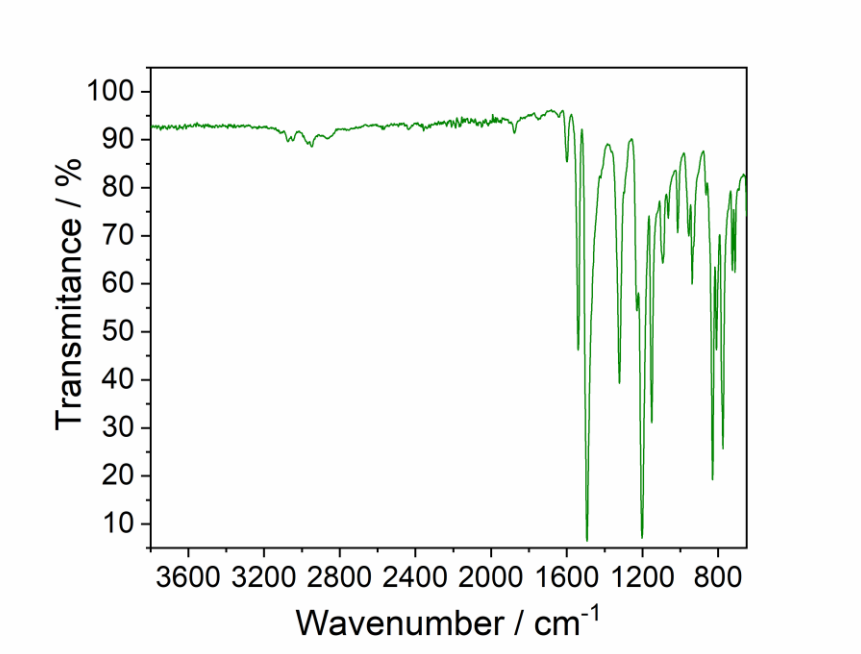

Fig. S7 Experimental infrared spectrum, in the range of 3800-650 cm^{-1}, of compound $[Ru_2Cl(D$*p*-$FPhF)_4]\cdot 0.5Et_2O$ (**4·0.5Et₂O**).

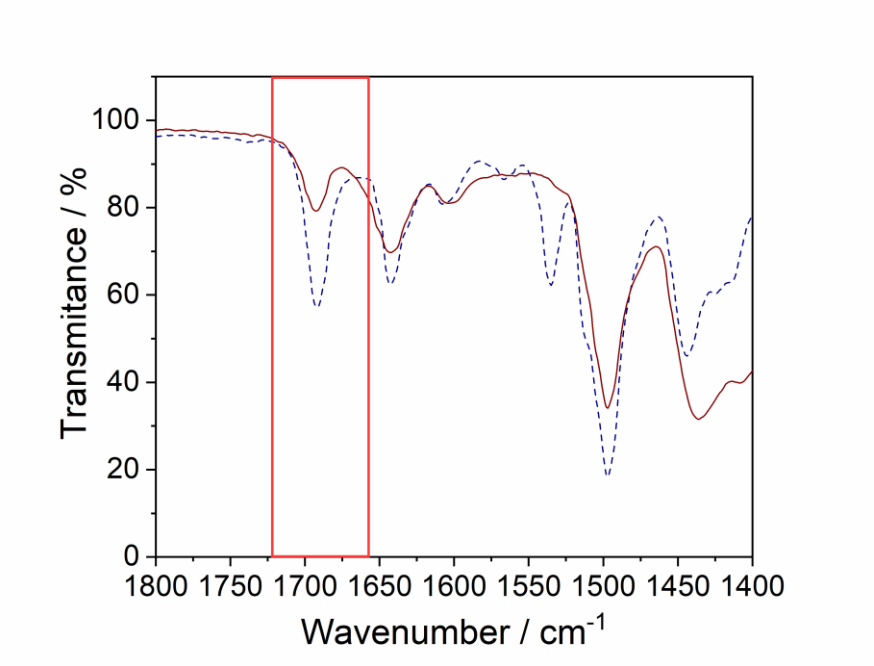

Fig. S8 Experimental infrared spectra, in the range of 1800-1400 cm^{-1}, of compounds $[Ru_2Cl(Dp\text{-}FPhF)(O_2CCH_3)_3(OCHNHC_6H_4F)]$ in wine red solid line, and $[Ru_2Cl(Dp\text{-}FPhF)_2(O_2CCH_3)_2(OCHNHC_6H_4F)]$ in navy blue dashed line. The bands centered around 1690 cm^{-1}, marked with a red box, appear when one of the axial positions is occupied by the ligand $OCHNHC_6H_4F$, derived from the formamidine hydrolysis.

MASS SPECTROMETRY

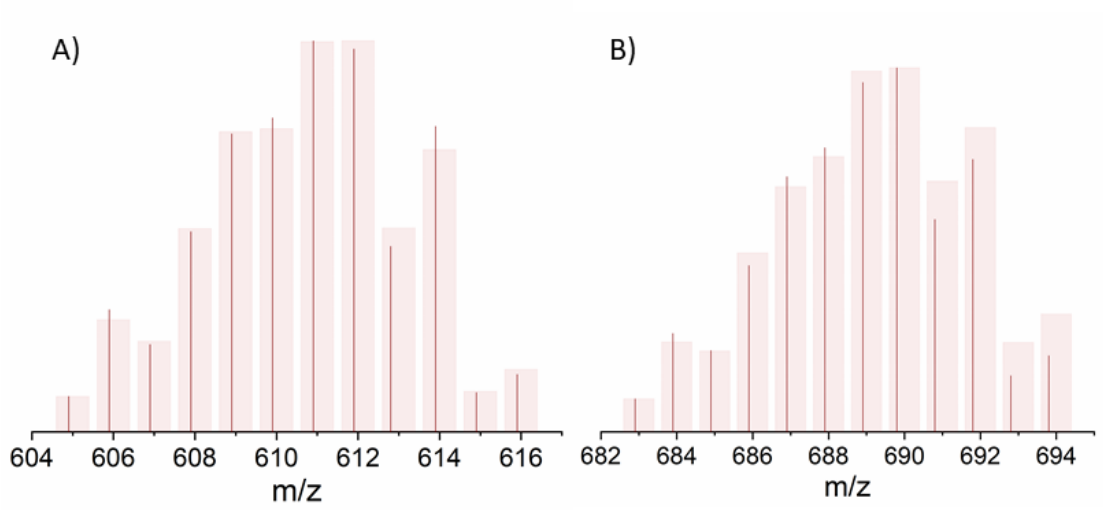

Fig. S9 Isotopic distribution in the positive ESI-MS spectrum of the A) [**1**-Cl]$^+$ and B) [**1**+CH_3CO]$^+$ species. Experimental results are represented in wine red lines, while the calculated isotopic distribution is in pale red bars.

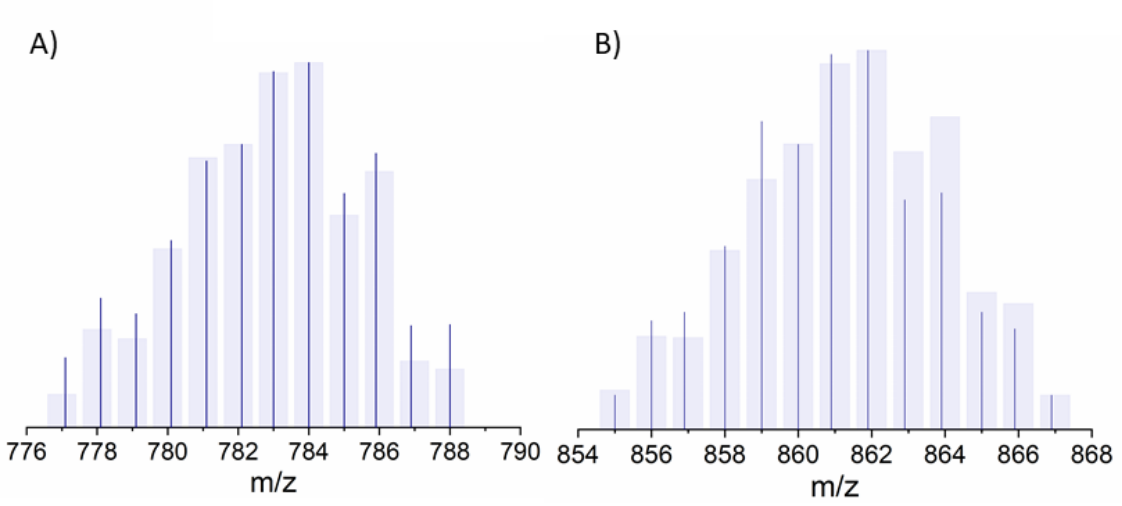

Fig. S10 Isotopic distribution in the positive ESI-MS spectrum of the a) [**2**-Cl]$^+$ and b) [**2**+CH_3CO]$^+$ species. Experimental results are represented in navy blue lines, while the calculated isotopic distribution is in pale blue bars.

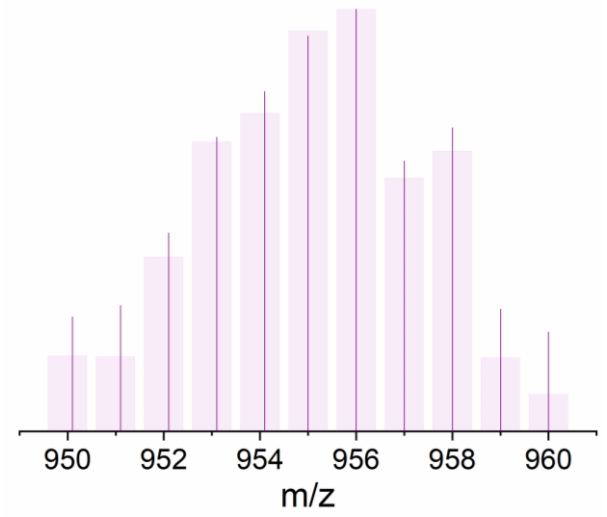

Fig. S11 Isotopic distribution in the positive ESI-MS spectrum of [**3**-Cl]$^+$. Experimental results are represented in purple lines, while the calculated isotopic distribution is in pale purple bars.

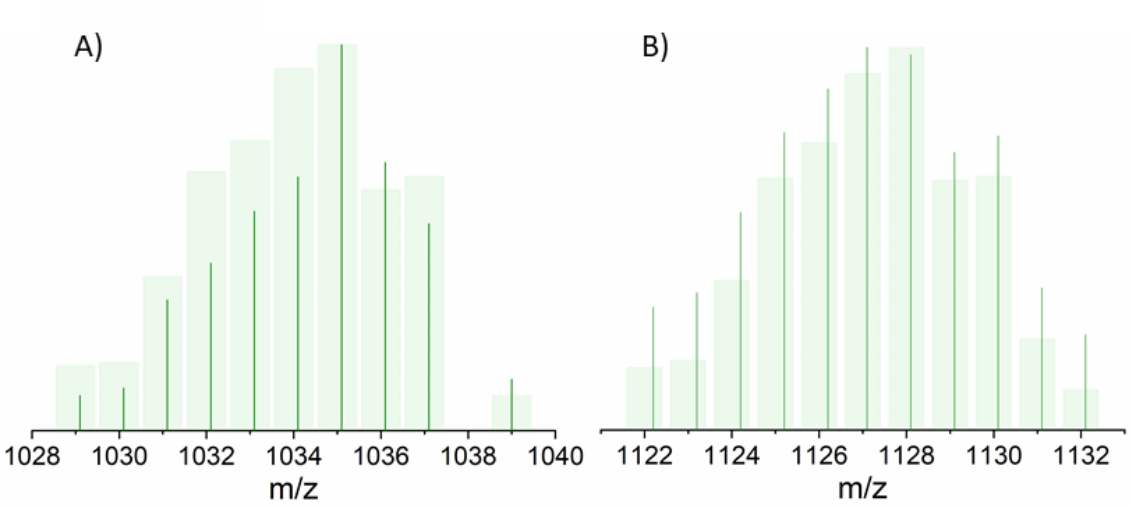

Fig. S12 Isotopic distribution in the positive ESI-MS spectrum of the a) [**4**-C_6H_4F+H]$^+$ and b) [**4**-Cl]$^+$ species. Experimental results are represented in olive green lines, while the calculated isotopic distribution is in pale green bars.

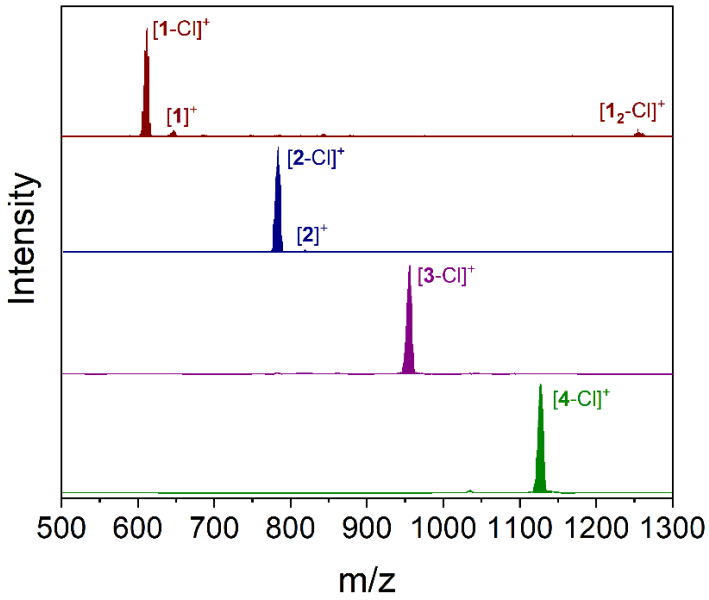

Fig. S13 MALDI mass spectra of compounds, from top to bottom, **1** (wine red), **2** (navy blue), **3** (purple) and **4** (olive green). Principal peaks are represented with their corresponding tentative assignment.

SINGLE CRYSTAL X-RAY DIFFRACTION

a) $[Ru_2Cl(Dp\text{-}FPhF)(O_2CCH_3)_3]_n \cdot 2CH_2Cl_2$ ($1_n \cdot 2CH_2Cl_2$) (CCDC 2122430)

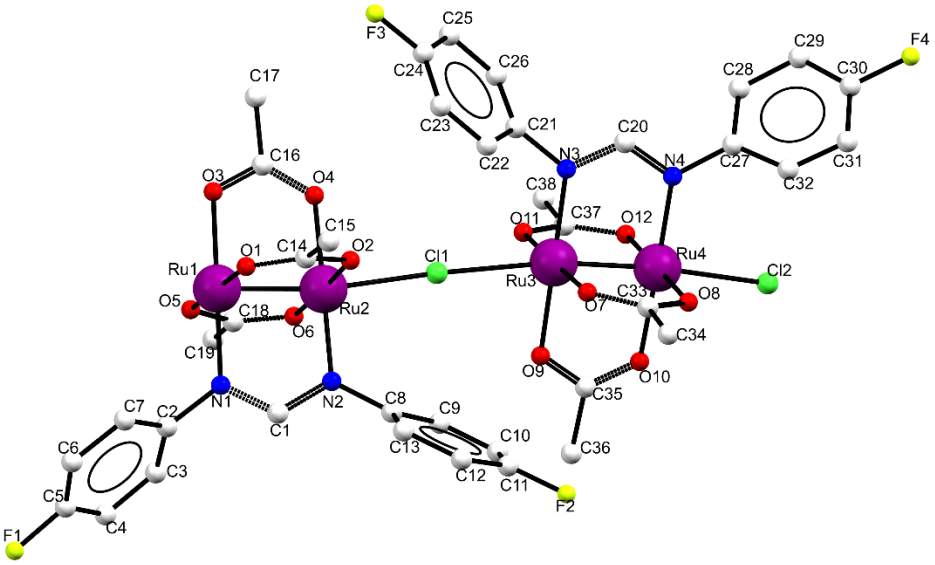

Fig. S14 Asymmetric unit of $\mathbf{1_n \cdot 2CH_2Cl_2}$. Hydrogen atoms and solvent molecules are omitted for clarity.

Table S1 Sample and crystal data for $\mathbf{1_n \cdot 2CH_2Cl_2}$.

Empirical formula	$C_{42}H_{44}Cl_{10}F_4N_4O_{12}Ru_4$
Formula weight/g·mol^{-1}	1631.59
Temperature/K	150(2)
Crystal system	triclinic
Space group	*P*-1
***a*/Å**	11.771(3)
***b*/Å**	14.742(4)
***c*/Å**	19.012(6)
α/°	112.09(2)
β/°	91.274(19)
γ/°	107.42(2)
Volume/Å^3	2882.6(15)
Z	2
ρ_{calc}/g cm^{-3}	1.880
μ/mm^1	1.563
F(000)	1604
Crystal size/mm^3	0.012 × 0.035 × 0.128
Radiation	MoK$_\alpha$ (λ = 0.71073)
Θ range for data collection/°	1.54 to 25.16
Index ranges	-14 ≤ h ≤ 14, -17 ≤ k ≤ 17, -22 ≤ l ≤22
Reflections collected	51319
Independent reflections	10604 [R_{int} = 0.1767]
Data/restraints/parameters	10604 / 646 / 692
Goodness-of-fit on F^2	0.975
Final R indexes [I>=2σ (I)]	R_1 = 0.1002, wR_2 = 0.2035
Final R indexes [all data]	R_1 = 0.2428, wR_2 = 0.2511
Largest diff. peak/hole / e Å^{-3}	1.572/-1.473

b) $[Ru_2Cl(Dp\text{-}FPhF)(O_2CCH_3)_3(DMSO)]\cdot 2CH_2Cl_2$ ($1DMSO\cdot 2CH_2Cl_2$) (CCDC 2153108)

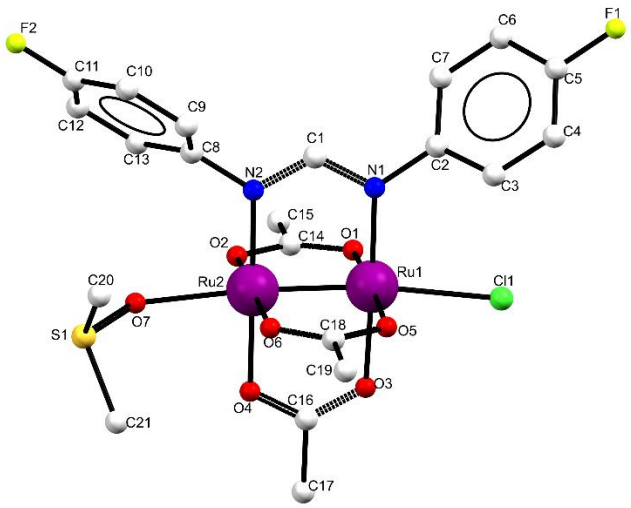

Fig. S15 Asymmetric unit of **$1DMSO\cdot 2CH_2Cl_2$**. Hydrogen atoms and solvent molecules are omitted for clarity.

Table S2 Sample and crystal data for **$1DMSO\cdot 2CH_2Cl_2$**.

Empirical formula	$C_{23}H_{28}Cl_5F_2N_2O_7Ru_2S$
Formula weight/g·mol^{-1}	893.92
Temperature/K	200
Crystal system	triclinic
Space group	*P*-1
***a*/Å**	11.4157(13)
***b*/Å**	11.6710(12)
***c*/Å**	13.1768(12)
α/°	73.119(4)
β/°	86.441(4)
γ/°	82.059(4)
Volume/Å^3	1663.4(3)
Z	2
ρ_{calc}/g cm^{-3}	1.785
μ/mm^1	1.425
F(000)	886
Crystal size/mm^3	0.233 × 0.05 × 0.013
Radiation	MoKα (λ = 0.71073)
Θ range for data collection/°	2.392 to 20.114
Index ranges	-13 ≤ h ≤ 13, -14 ≤ k ≤ 14, -15 ≤ l ≤15
Reflections collected	26102
Independent reflections	6066 [R_{int} = 0.1831]
Data/restraints/parameters	6066 / 0 / 384
Goodness-of-fit on F^2	0.968
Final R indexes [I>=2σ (I)]	R_1 = 0.0438, wR_2 = 0.0715
Final R indexes [all data]	R_1 = 0.0953, wR_2 = 0.0853
Largest diff. peak/hole / e Å^{-3}	0.595 / -0.582

c) $[Ru_2Cl(Dp\text{-}FPhF)_2(O_2CCH_3)_2(OH_2)]\cdot 2H_2O$ ($2H_2O\cdot 2H_2O$) (CCDC 2122431)

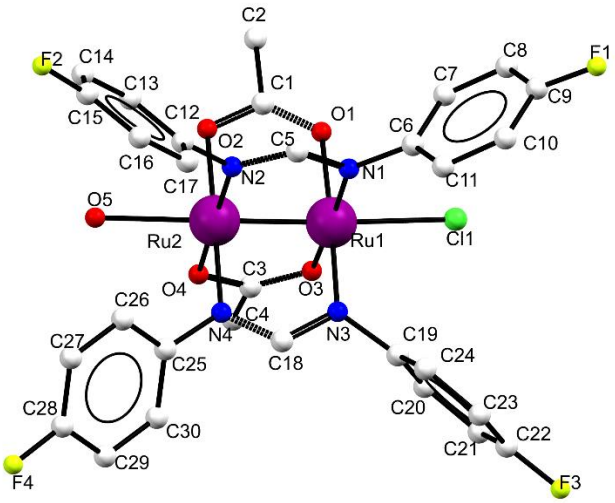

Fig. S16 Asymmetric unit of **$2H_2O\cdot 2H_2O$**. Hydrogen atoms and solvent molecules are omitted for clarity.

Table S3 Sample and crystal data for **$2H_2O\cdot 2H_2O$**.

Empirical formula	$C_{30}H_{30}ClF_4N_4O_7Ru_2$
Formula weight/g·mol^{-1}	872.17
Temperature/K	296(2)
Crystal system	orthorhombic
Space group	$P2_12_12_1$
***a*/Å**	13.612(2)
***b*/Å**	14.755(2)
***c*/Å**	17.022(3)
α/°	90
β/°	90
γ/°	90
Volume/Å^3	3418.8(9)
Z	4
ρ_{calc}/g cm^{-3}	1.694
μ/mm^1	1.033
F(000)	1740
Crystal size/mm^3	0.25 × 0.12 × 0.12
Radiation	MoKα (λ = 0.71073)
2Θ range for data collection/°	1.83 to 23.26
Index ranges	-12 ≤ h ≤ 15, -16 ≤ k ≤ 16, -18 ≤ l ≤ 18
Reflections collected	9101
Independent reflections	4650 [R_{int} = 0.0986]
Data/restraints/parameters	4650 / 204 / 357
Goodness-of-fit on F^2	1.092
Final R indexes [I>=2σ (I)]	R_1 = 0.0938, wR_2 = 0.1811
Final R indexes [all data]	R_1 = 0.2056, wR_2 = 0.2402
Largest diff. peak/hole / e Å^{-3}	1.063 / -1.077
Flack parameter	0.08(10)

d) $[Ru_2Cl(Dp\text{-}FPhF)_3(O_2CCH_3)]\cdot 1.5CH_2Cl_2$ (3·1.5CH_2Cl_2) (CCDC 2122432)

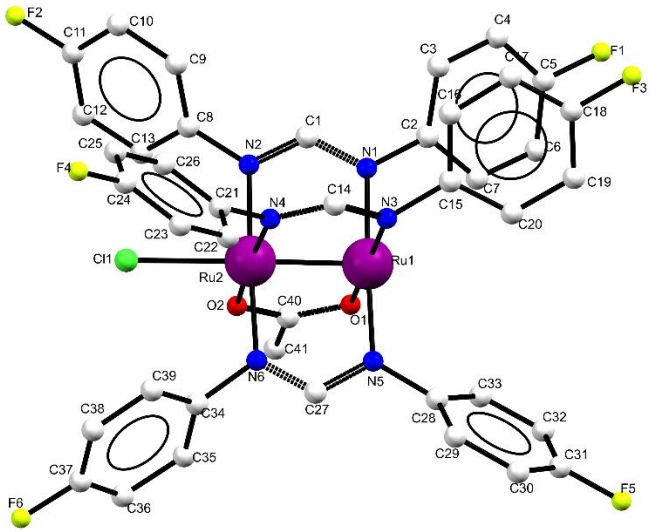

Fig. S17 Asymmetric unit of **3·1.5CH_2Cl_2**. Hydrogen atoms and solvent molecules are omitted for clarity.

Table S4 Sample and crystal data for **3·1.5CH_2Cl_2**.

Empirical formula	$C_{42.5}H_{33}Cl_4F_6N_6O_2Ru_2$
Formula weight/g·mol^{-1}	1117.69
Temperature/K	200(2)
Crystal system	monoclinic
Space group	*C*2/*c*
***a*/Å**	41.5237(13)
***b*/Å**	12.0831 (4)
***c*/Å**	20.6065(5)
α/°	90
β/°	114.251(1)
γ/°	90
Volume/Å^3	9426.6(5)
Z	8
ρ_{calc}/g cm^{-3}	1.575
μ/mm^1	0.933
F(000)	4448
Crystal size/mm^3	0.030 × 0.040 × 0.130
Radiation	MoKα (λ = 0.71073)
Θ range for data collection/°	1.77 to 25.35
Index ranges	-50 ≤ h ≤ 50, -14 ≤ k ≤ 14, -24 ≤ l ≤ 24
Reflections collected	78266
Independent reflections	8625 [R_{int} = 0.0588]
Data/restraints/parameters	8625 / 12 / 592
Goodness-of-fit on F^2	1.164
Final R indexes [I>=2σ (I)]	R_1 = 0.0588, wR_2 = 0.1769
Final R indexes [all data]	R_1 = 0.0800, wR_2 = 0.1938
Largest diff. peak/hole / e Å^{-3}	2.614 / -0.901

e) $[Ru_2Cl(D\textit{p}\text{-}FPhF)_4]\cdot CHCl_3$ ($4\cdot CHCl_3$) (CCDC 2122433)

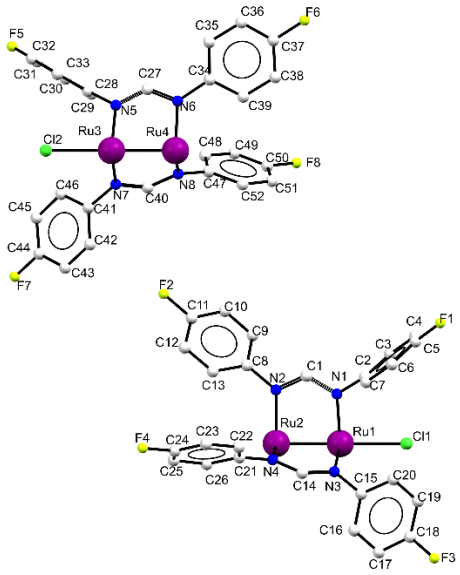

Fig. S18 Asymmetric unit of **$4\cdot CHCl_3$**. Hydrogen atoms and solvent molecules are omitted for clarity.

Table S5 Sample and crystal data for of **$4\cdot CHCl_3$**.

Empirical formula	$C_{53}H_{37}Cl_4F_8N_8Ru_2$
Formula weight/g·mol^{-1}	1281.84
Temperature/K	250(2)
Crystal system	monoclinic
Space group	*C*2/*c*
***a*/Å**	27.5579(11)
***b*/Å**	22.4236(10)
***c*/Å**	21.5762(14)
α/°	90
β/°	129.5250(10)
γ/°	90
Volume/Å^3	10284.3(9)
Z	8
ρ_{calc}/g cm^{-3}	1.656
μ/mm^1	0.871
F(000)	5112
Crystal size/mm^3	0.213 × 0.034 × 0.022
Radiation	Mo Kα (λ = 0.71073)
2Θ range for data collection/°	1.32 to 25.35
Index ranges	-33 ≤ h ≤ 33, -26 ≤ k ≤ 26, -25 ≤ l ≤ 25
Reflections collected	155149
Independent reflections	9369 [R_{int} = 0.0951]
Data/restraints/parameters	9369 / 0 / 677
Goodness-of-fit on F^2	1.000
Final R indexes [I>=2σ (I)]	R_1 = 0.0435, wR_2 = 0.0910
Final R indexes [all data]	R_1 = 0.0923, wR_2 = 0.1134
Largest diff. peak/hole / e Å^{-3}	1.448 / -1.332

f) $[Ru_2Cl(Dp\text{-}FPhF)(O_2CCH_3)_3(OCHNHC_6H_4F)]\cdot 0.25CH_2Cl_2\cdot H_2O$ (CCDC 2122434)

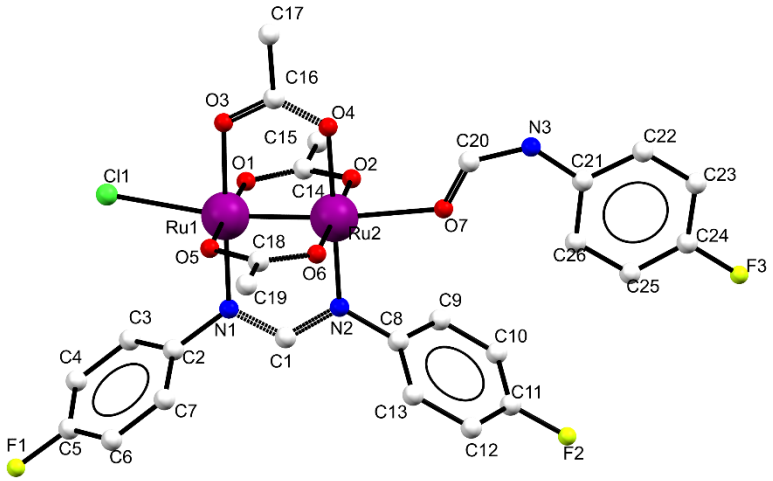

Fig. S19 Asymmetric unit of $[Ru_2Cl(OCHNHC_6H_4F)(Dp\text{-}FPhF)(O_2CCH_3)_3]\cdot 0.25CH_2Cl_2\cdot H_2O$. Hydrogen atoms and solvent molecules are omitted for clarity.

Table S6 Sample and crystal data for $[Ru_2Cl(OCHNHC_6H_4F)(Dp\text{-}FPhF)(O_2CCH_3)_3]\cdot 0.25CH_2Cl_2\cdot H_2O$

Empirical formula	$C_{26.25}H_{26.50}Cl_{1.50}F_3N_3O_8Ru_2$
Formula weight/g·mol^{-1}	824.32
Temperature/K	296(2)
Crystal system	trigonal
Space group	*R*-3
***a*/Å**	39.2728(12)
***b*/Å**	39.2728(12)
***c*/Å**	10.8904(4)
α/°	90
β/°	90
γ/°	120
Volume/Å^3	14546.5(10)
Z	18
ρ_{calc}/g cm^{-3}	1.694
μ/mm^1	1.125
F(000)	7371
Crystal size/mm^3	0.278 × 0.079 × 0.068
Radiation	MoKα (λ = 0.71073)
2Θ range for data collection/°	1.96 to 25.35
Index ranges	-47 ≤ h ≤ 47, -47 ≤ k ≤ 47, -13 ≤ l ≤ 13
Reflections collected	138955
Independent reflections	5898 [R_{int} = 0.1082]
Data/restraints/parameters	5898 / 2 / 402
Goodness-of-fit on F^2	1.048
Final R indexes [I>=2σ (I)]	R_1 = 0.0386, wR_2 = 0.1157
Final R indexes [all data]	R_1 = 0.0601, wR_2 = 0.1282
Largest diff. peak/hole / e Å^{-3}	1.274 / -0.513

g) $(Et_3NH)[Ru_2Cl_2(Dp\text{-}FPhF)(O_2CCH_3)_3]\cdot 0.5CH_2Cl_2$ (CCDC 2122435)

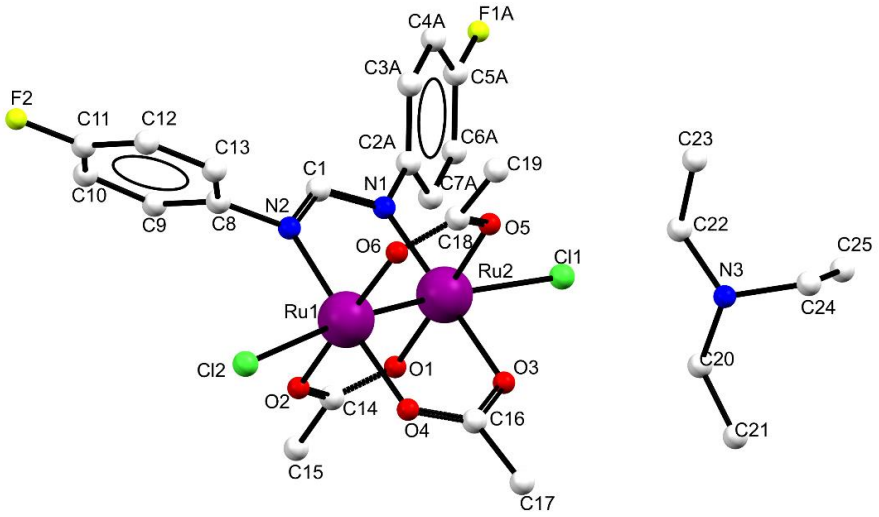

Fig. S20 Asymmetric unit of $(Et_3NH)[Ru_2Cl_2(Dp\text{-}FPhF)(O_2CCH_3)_3]\cdot 0.5CH_2Cl_2$. Hydrogen atoms and solvent molecules are omitted for clarity. Only one of the alternative set of positions of the disordered fragment is depicted.

Table S7 Sample and crystal data for $(Et_3NH)[Ru_2Cl_2(Dp\text{-}FPhF)(O_2CCH_3)_3]\cdot 0.5CH_2Cl_2$.

Empirical formula	$C_{25.5}H_{35}Cl_3F_2N_3O_6Ru_2$
Formula weight/g·mol^{-1}	826.05
Temperature/K	296(2)
Crystal system	monoclinic
Space group	*C*2/*c*
***a*/Å**	19.3249(5)
***b*/Å**	13.3413(3)
***c*/Å**	27.2352(7)
α/°	90
β/°	91.3830(10)
γ/°	90
Volume/Å^3	7019.7(3)
Z	8
ρ_{calc}/g cm^{-3}	1.563
μ/mm^1	1.138
F(000)	3312
Crystal size/mm^3	0.128 × 0.114 × 0.033
Radiation	MoKα (λ = 0.71073)
2Θ range for data collection/°	2.62 to 25.35
Index ranges	-23 ≤ h ≤ 23, -16 ≤ k ≤ 16, -32 ≤ l ≤ 32
Reflections collected	119246
Independent reflections	6402 [R_{int} = 0.0574]
Data/restraints/parameters	6402 / 212 / 379
Goodness-of-fit on F^2	1.069
Final R indexes [I>=2σ (I)]	R_1 = 0.0608, wR_2 = 0.1550
Final R indexes [all data]	R_1 = 0.0757, wR_2 = 0.1668
Largest diff. peak/hole / e Å^{-3}	2.666 / -2.776

h) $[Ru_2Cl(Dp\text{-}FPhF)_2(O_2CCH_3)_2(OCHNHC_6H_4F)]$ (CCDC 2122436)

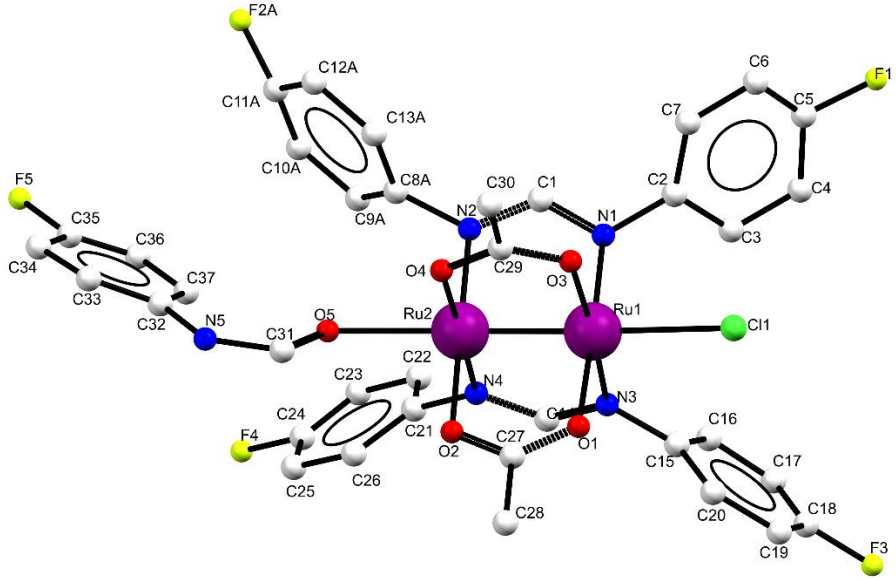

Fig. S21 Asymmetric unit of $[Ru_2Cl(Dp\text{-}FPhF)_2(O_2CCH_3)_2(OCHNHC_6H_4F)]$. Hydrogen atoms are omitted for clarity. Only one of the alternative set of positions of the disordered fragment is depicted.

Table S8 Sample and crystal data for $[Ru_2Cl(Dp\text{-}FPhF)_2(O_2CCH_3)_2(OCHNHC_6H_4F)]$.

Empirical formula	$C_{37}H_{30}ClF_5N_5O_5Ru_2$
Formula weight/g·mol^{-1}	957.25
Temperature/K	296(2)
Crystal system	orthorhombic
Space group	$P2_12_12_1$
***a*/Å**	14.2365(8)
***b*/Å**	16.2626(9)
***c*/Å**	16.8307(9)
α/°	90
β/°	90
γ/°	90
Volume/Å^3	3896.7(4)
Z	4
ρ_{calc}/g cm^{-3}	1.632
μ/mm^1	0.916
F(000)	1908
Crystal size/mm^3	0.260 × 0.170 × 0.170
Radiation	MoKα (λ = 0.71073)
2Θ range for data collection/°	1.74 to 25.35
Index ranges	-17 ≤ h ≤ 17, -19 ≤ k ≤ 19, -20 ≤ l ≤ 20
Reflections collected	33628
Independent reflections	7116 [R_{int} = 0.0634]
Data/restraints/parameters	7116 / 612 / 472
Goodness-of-fit on F^2	1.087
Final R indexes [I>=2σ (I)]	R_1 = 0.0566, wR_2 = 0.1197
Final R indexes [all data]	R_1 = 0.1022, wR_2 = 0.1495
Largest diff. peak/hole / e Å^{-3}	0.898/ -1.030
Flack parameter	-0.05(2)

i) C-H···F contacts in $1_n \cdot 2CH_2Cl_2$, $1DMSO \cdot 2CH_2Cl_2$, $2H_2O \cdot 2H_2O$, $3 \cdot 1.5CH_2Cl_2$ and $4 \cdot CHCl_3$

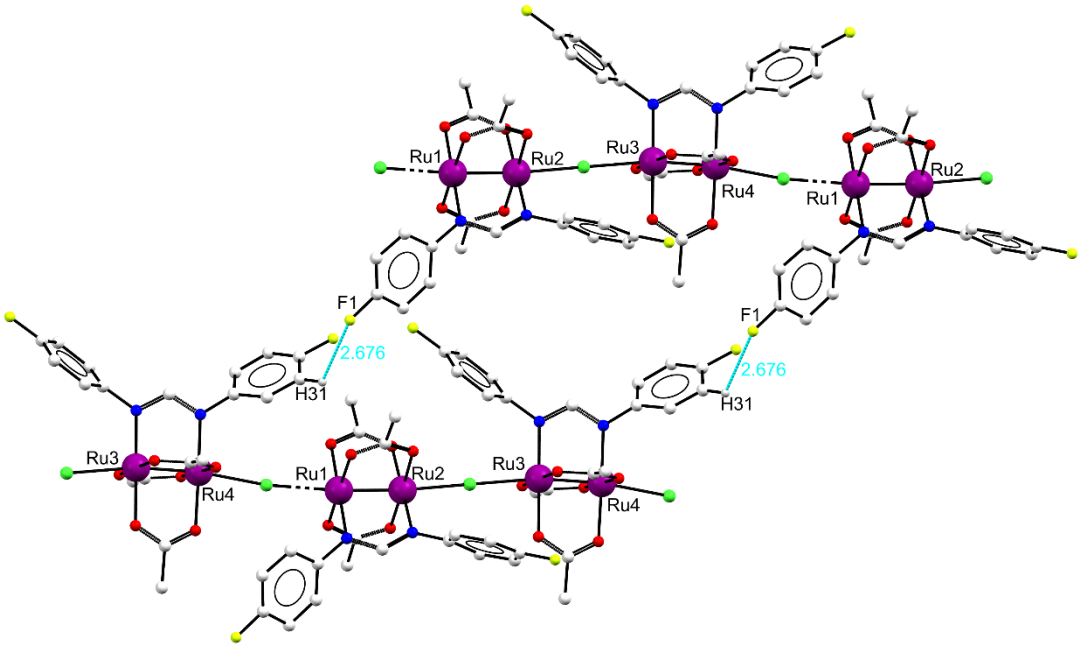

Fig. S22 C-H···F contacts between neighbour chains in the structure of **$1_n \cdot 2CH_2Cl_2$**. Distances (Å) are shown in blue.

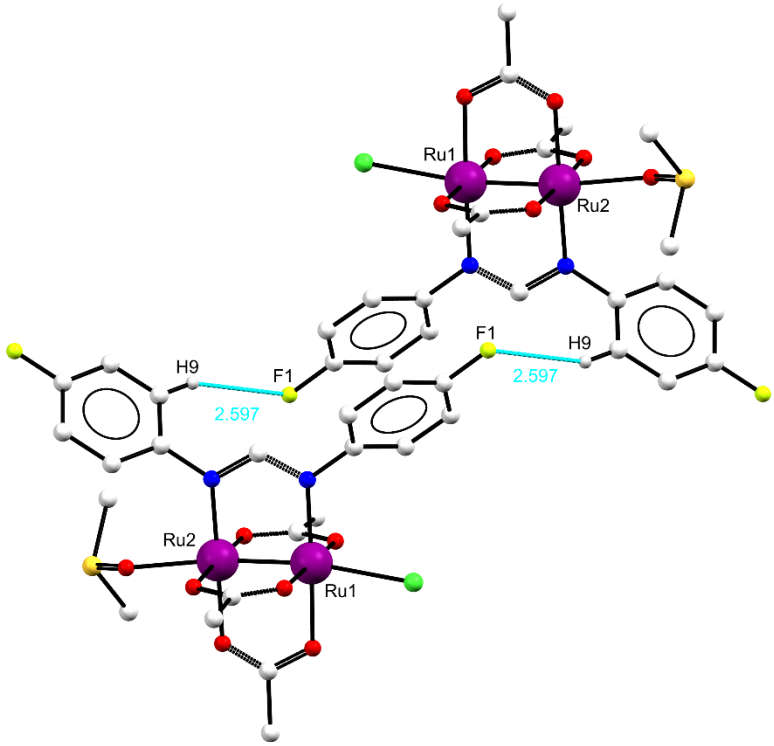

Fig. S23 C-H···F contacts between neighbour chains in the structure of **$1DMSO \cdot 2CH_2Cl_2$**. Distances (Å) are shown in blue.

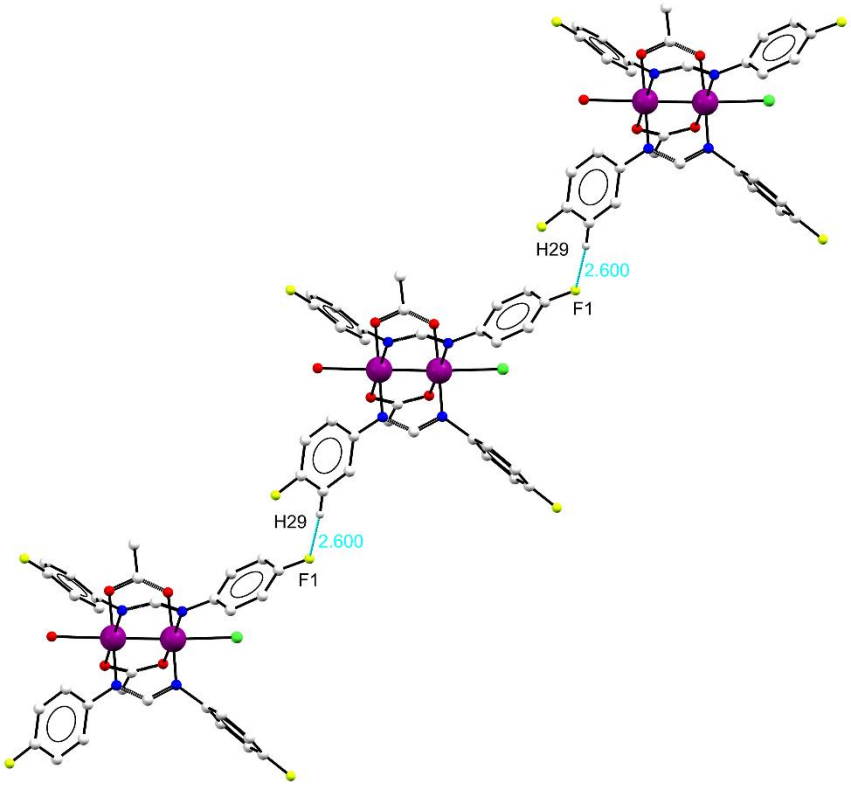

Fig. S24 C-H···F contacts between neighbour paddlewheel molecules in the structure of **$2H_2O \cdot 2H_2O$**. Distances (Å) are shown in blue.

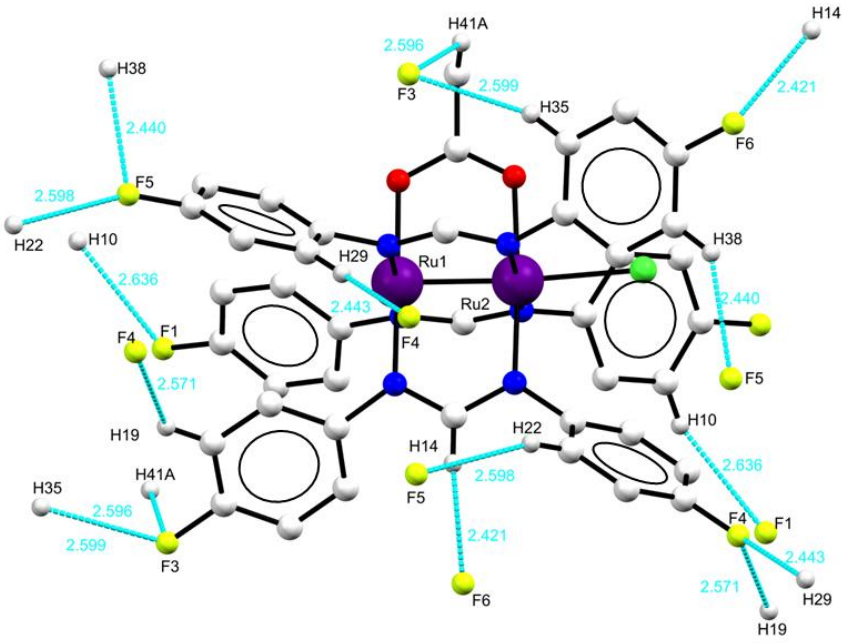

Fig. S25 C-H···F contacts between neighbour paddlewheel molecules in the structure of **$3 \cdot 1.5CH_2Cl_2$**. Distances (Å) are shown in blue.

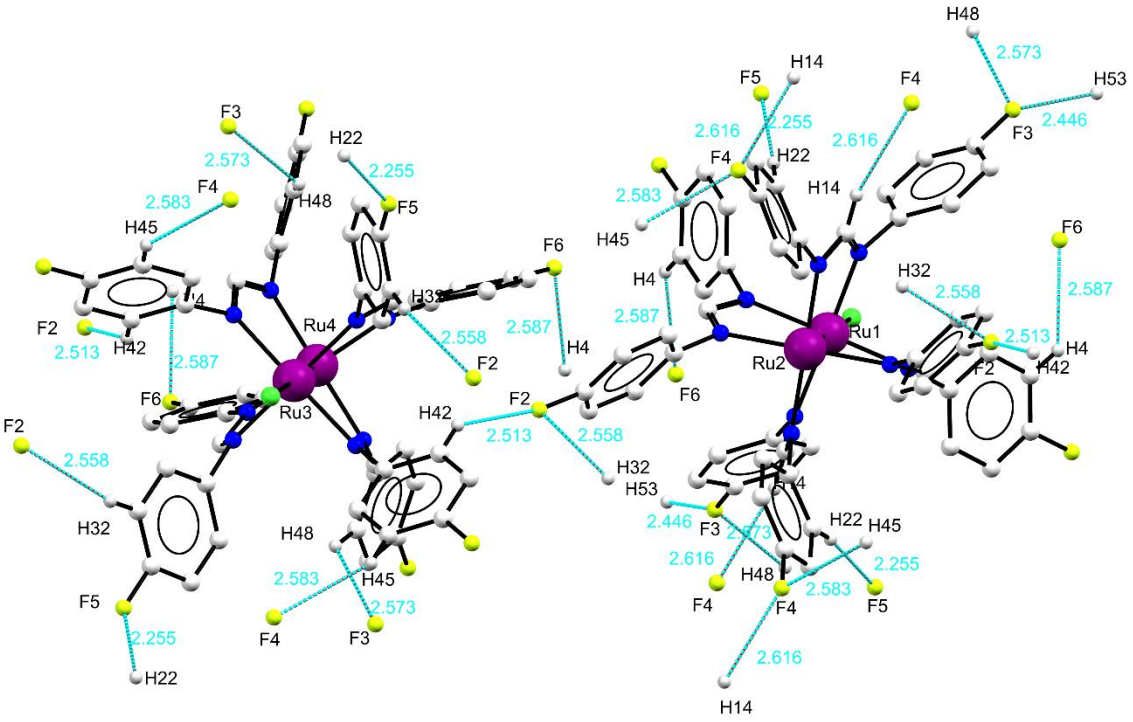

Fig. S26 C-H···F contacts of Ru1Ru2 (top) and Ru3Ru4 (down) units with neighbour paddlewheel molecules in the structure of **4·CHCl$_3$**. Distances (Å) are shown in blue.

MAGNETIC MEASUREMENTS

The equations of Cukiernik's model,[9] based on the equations of Telser and Drago,[10,11] which were used for fitting the magnetic data of compounds **1** – **4**, are the following:

$$\chi' = \frac{\chi'_M}{1 - \chi'_M \left(\frac{2zJ'}{Ng^2\beta^2} \right)}$$

Equation S1

$$\chi'_M = \chi_M + TIP$$

Equation S2

$$\chi_M = \frac{\chi_{\parallel} + 2\chi_{\perp}}{3}$$

Equation S3

Where $\chi_{\parallel}$ and $\chi_{\perp}$ are the parallel and perpendicular contributions to the magnetic susceptibility and are defined by equations S4 and S5.

$$\chi_{\parallel} = \frac{Ng^2\beta^2}{kT} \left[\frac{1 + 9e^{-2D/kT}}{4\left(1 + e^{-2D/kT}\right)} \right]$$

Equation S4

$$\chi_{\perp} = \frac{Ng^2\beta^2}{kT} \left[\frac{4 + \left(\frac{3kT}{D} \right)\left(1 - e^{-2D/kT}\right)}{4(1 + e^{-2D/kT})} \right]$$

Equation S5

In this model, *N*, *g*, β, and *k* have their usual meanings. These equations yielded good agreements between the experimental and calculated curves of molar susceptibility and $\chi_M T$ (Fig. S27-S30).

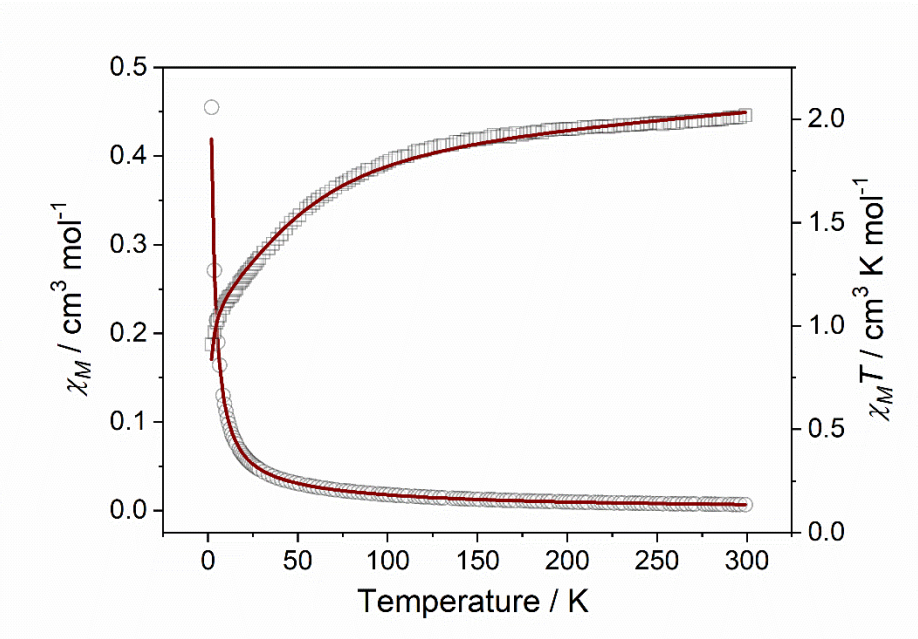

Fig. S27 Variable temperature molar susceptibility χ_M (circles) and $\chi_M T$ (squares) for complex [Ru_2Cl(D*p*-FPhF)$(O_2CCH_3)_3(OH_2)$] (**$1H_2O$**). Wine red solid lines are the result of the best fit to the model described in the text.

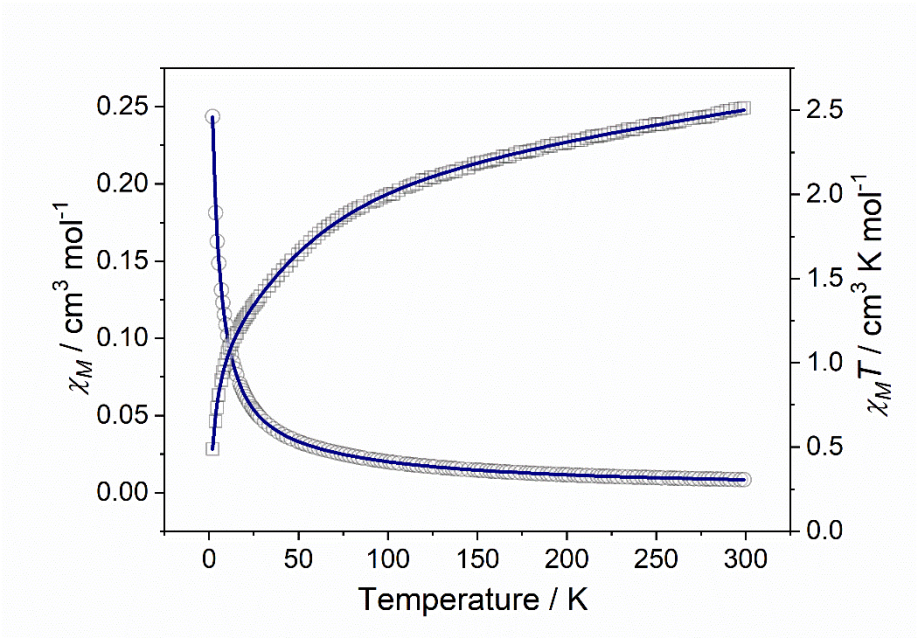

Fig. S28 Variable temperature molar susceptibility χ_M (circles) and $\chi_M T$ (squares) for complex [Ru_2Cl(D*p*-FPhF)$_2(O_2CCH_3)_2(OH_2)]\cdot 0.5H_2O$ (**$2H_2O\cdot 0.5H_2O$**). Navy blue solid lines are the result of the best fit to the model described in the text.

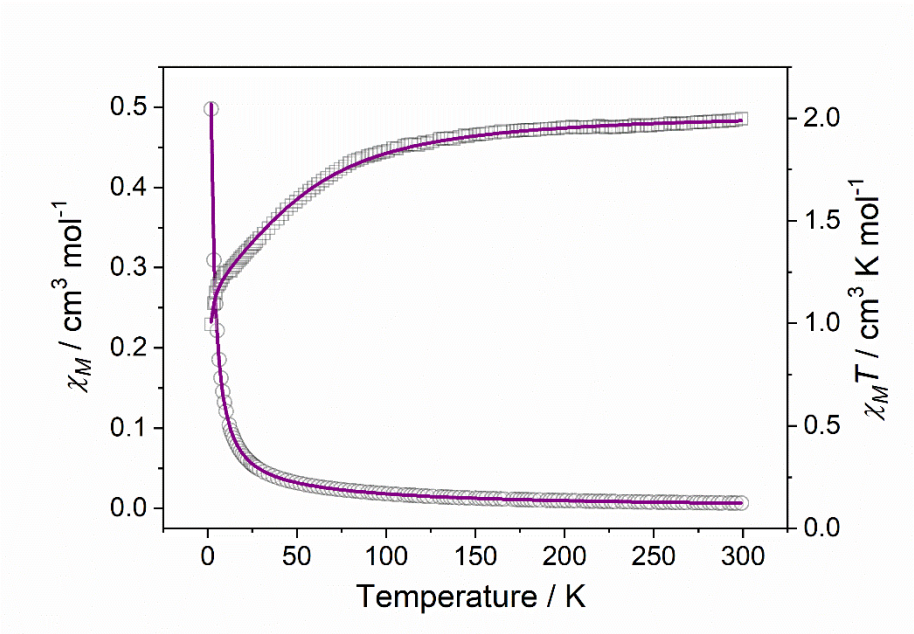

Fig. S29 Variable temperature molar susceptibility χ_M (circles) and $\chi_M T$ (squares) for complex [Ru_2Cl(D*p*-FPhF)$_3$(O_2CCH_3)]·0.5Et_2O (**3·0.5Et_2O**). Purple solid lines are the result of the best fit to the model described in the text.

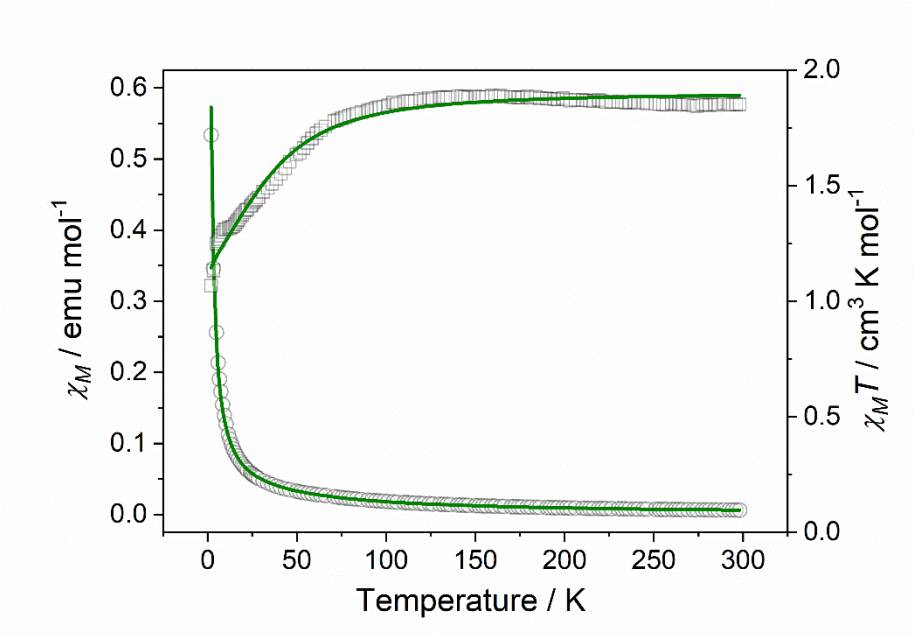

Fig. S30 Variable temperature molar susceptibility χ_M (circles) and $\chi_M T$ (squares) for complex [Ru_2Cl(D*p*-FPhF)$_4$]·0.5Et_2O (**4·0.5Et_2O**). Olive green solid lines are the result of the best fit to the model described in the text.

Table S9 Magnetic parameters obtained from the fit of the experimental magnetic data of compounds **1** – **4**. σ^2 indicates the quality of the fits.

Compound	*g*	*D* cm^{-1}	*zJ* cm^{-1}	*TIP* $cm^3 \cdot mol^{-1}$	$\sigma^2 \cdot 10^5$
$[Ru_2Cl(Dp\text{-}FPhF)(O_2CCH_3)_3(OH_2)]$ (**1H₂O**)	2.00	60.39	-0.33	6.17×10^{-4}	3.49
$[Ru_2Cl(Dp\text{-}FPhF)_2(O_2CCH_3)_2(OH_2)]$ (**2H₂O**)	2.14	62.40	-1.53	1.47×10^{-3}	0.53
$[Ru_2Cl(Dp\text{-}FPhF)_3(O_2CCH_3)]$ (**3**)	2.02	61.54	-0.18	7.11×10^{-5}	0.90
$[Ru_2Cl(Dp\text{-}FPhF)_4]$ (**4**)	2.00	45.00	0.00	1.32×10^{-7}	9.35

$\sigma^2 = \Sigma(\mu_{\text{eff. calcd.}} - \mu_{\text{eff. exp.}})^2/\Sigma\mu_{\text{eff. exp.}}^2$

CYCLIC VOLTAMMETRY

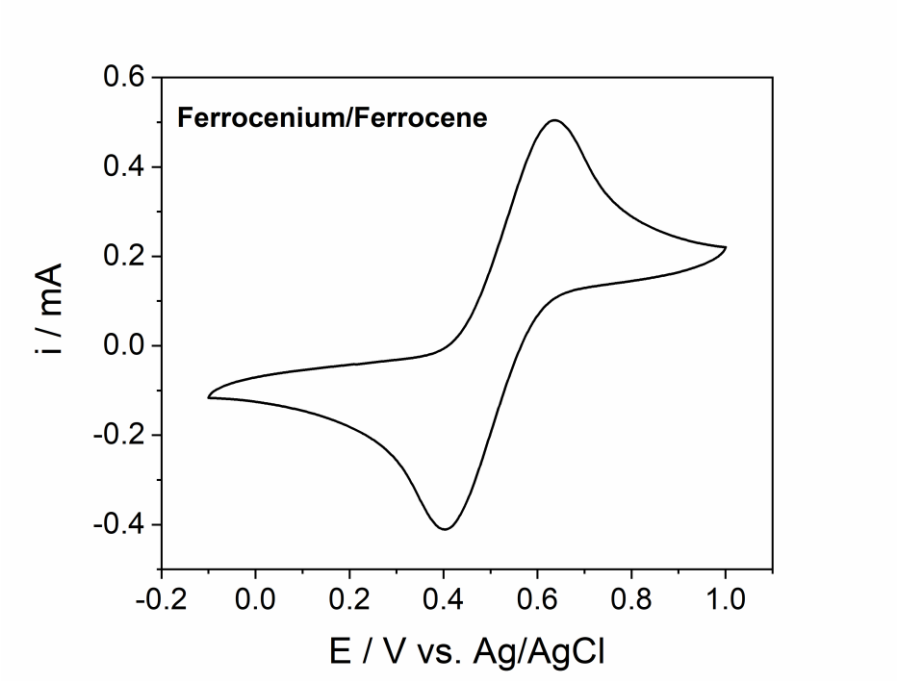

Fig. S31 Cyclic voltammogram of the ferrocenium/ferrocene couple, measured in a 0.1 M TBAP solution in dichloromethane.

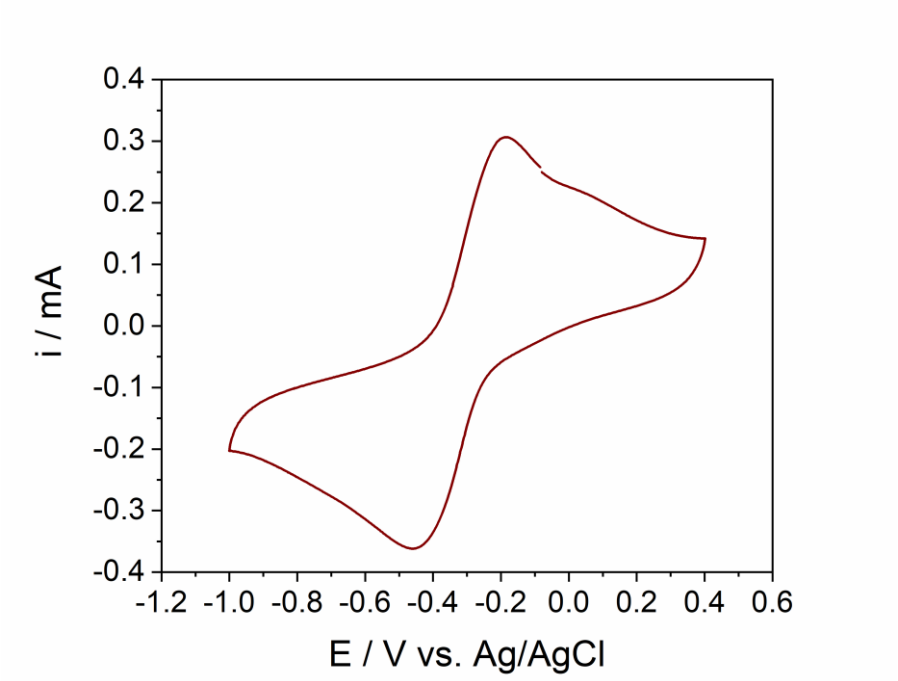

Fig. S32 Cyclic voltammogram of compound **1**, measured in a 0.1 M KCl solution in water at 25 ^{o}C.

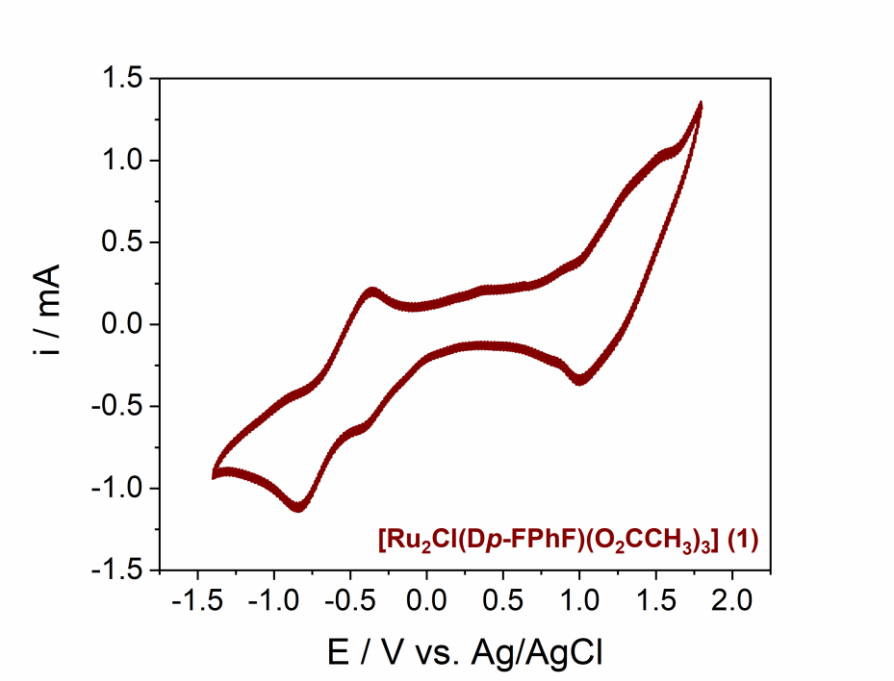

Fig. S33 Cyclic voltammogram of compound **1**, measured in a 0.1 M TBAP solution in dichloromethane at 25 °C.

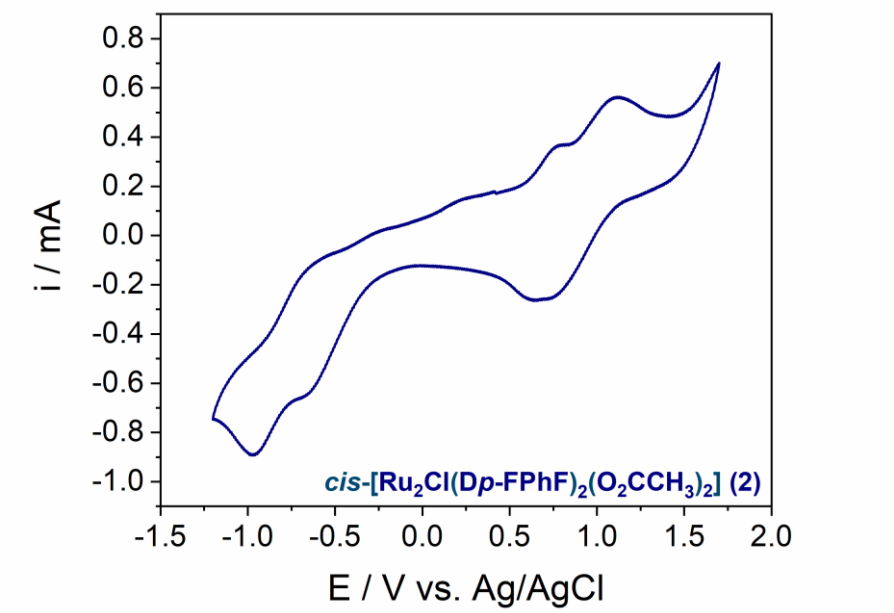

Fig. S34 Cyclic voltammogram of compound **2**, measured in a 0.1 M TBAP solution in dichloromethane at 25 °C.

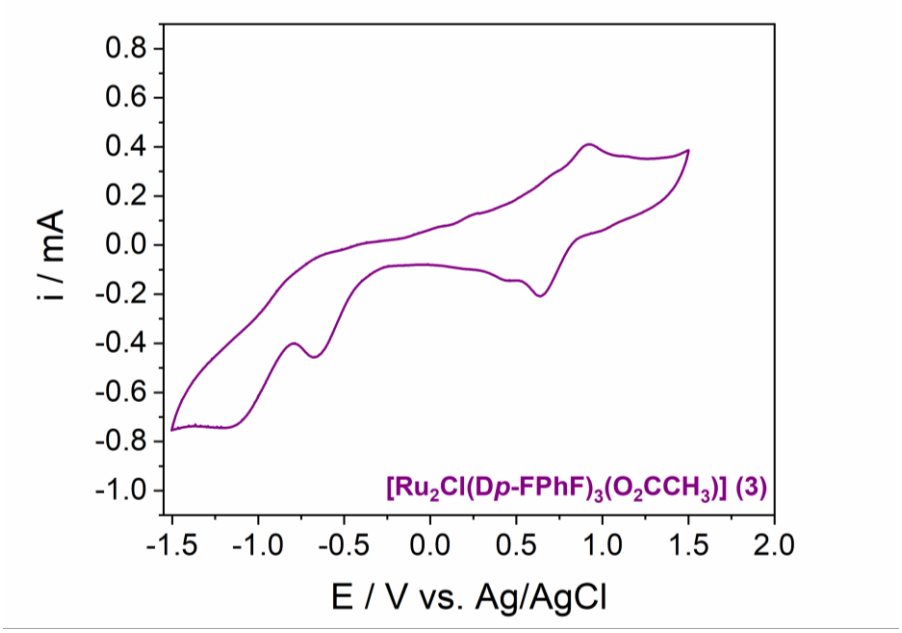

Fig. S35 Cyclic voltammogram of compound **3**, measured in a 0.1 M TBAP solution in dichloromethane at 25 °C.

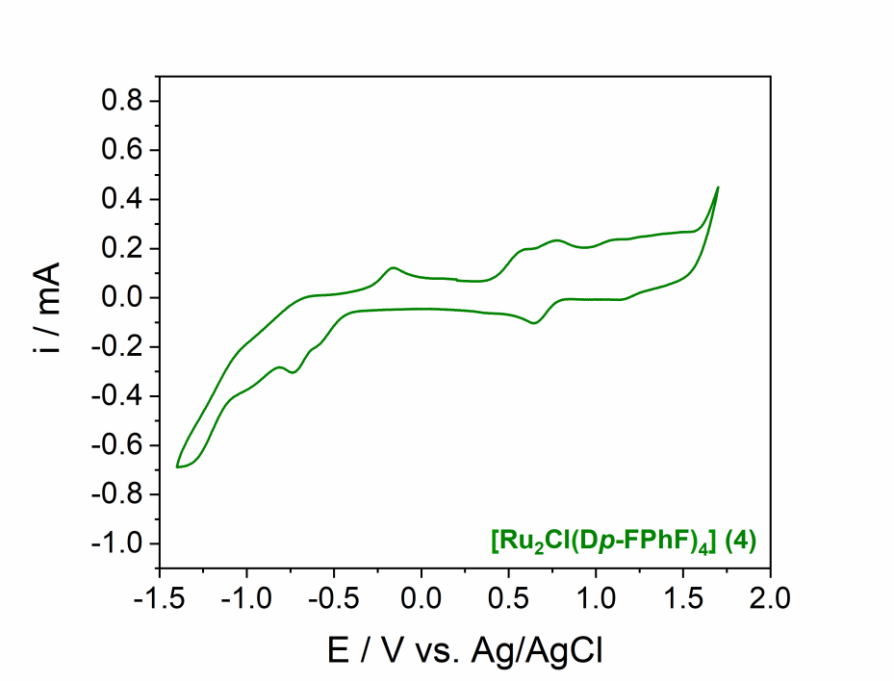

Fig. S36 Cyclic voltammogram of compound **4**, measured in a 0.1 M TBAP solution in dichloromethane at 25 °C.

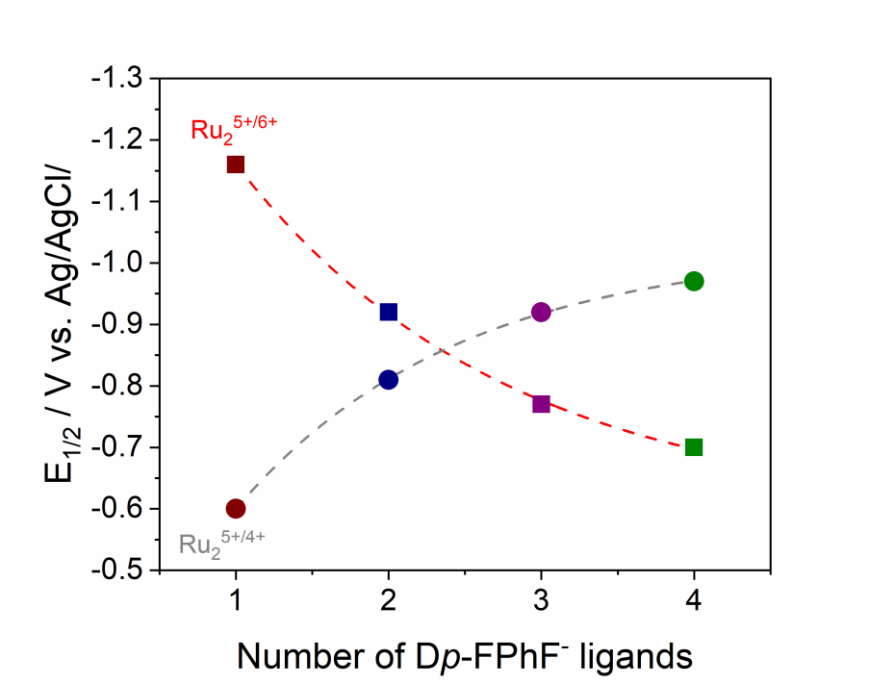

Fig. S37 Reduction half-wave potentials for the Ru_2^{5+}/Ru_2^{6+} oxidation (squares, red dashed line), and Ru_2^{5+}/Ru_2^{4+} reduction (circles, grey dashed line) processes. Data obtained from the CVs of compounds **1** (wine red), **2** (navy blue), **3** (purple) and **4** (olive green), measured in a 0.1 M TBAP solution in dichloromethane at 25 ^{o}C.

^{1}H and ^{19}F-NMR SPECTROSCOPY

^{1}H-NMR spectra (measured in a diluted solution in CD_2Cl_2 at 25 ^{o}C) of compounds **1** – **4** are shown in Fig. S38, while the assignment and chemical shifts of the protons are resumed in Table S10. The results are consistent with the literature.[4,12]

In the case of complex **1**, there are two chemically different acetate protons, whether they are in a *cis* (six protons) or *trans* (three protons) position with respect to D*p*-FPhF^{-}. Two sharp signals with different intensities assigned to these groups can be found, centred at -35.2 (*cis*, **e**) and -24.3 (*trans*, **d**) ppm. In the spectrum of compound **2**, only one signal (**d**) at -20.5 ppm is found, since both -CH_3 groups are chemically equivalent. This is due to the *cis* configuration of the molecule, previously confirmed with X-ray measurements. Only one signal (-18.4 ppm, **d**) is found in the spectrum of complex **3**, as there is just one acetate in the structure. No signal is detectable in the spectrum of **4** due to the absence of this ligand.

In the case of the formamidinate ligands, several signals corresponding to CH groups can be found. The aliphatic protons are chemically equivalent in compounds **1**, **2** and **4**, being represented as one broad and low signal (**a**), with a large paramagnetic shift. These are centred at -71.3, -83.5 and -23.2 ppm, respectively. In compound **3**, two different groups can be noticed, whether they are in a *cis* (-52.3 ppm, **e**) or *trans* (-72.8 ppm, **a**) position with respect to the carboxylate ligand.

Nevertheless, the interpretation of the proton signals corresponding to the aromatic groups is not straightforward. Two chemically differentiated aromatic protons, depending on their position with respect to the axial Cl ligand, can be distinguished. The *ortho*-H are more affected by the chloride than the *meta*-H, as the two split signals are more separated. *Ortho*- protons (**c**) are centred at -20.2 and -8.5 ppm for **1**, -21.3 and -2.22 ppm for **2**, and -13.2 and 8.8 ppm for **4**, while *meta*- (**b**) can be found around 20.2 and 22.2 ppm for **1**, 15.9 and 17.9 ppm for **2**, and 12.2 and 13.3 ppm for **4**. In the case of complex **3**, the *cis* or *trans* configuration also provokes differences in chemical shifts, giving rise to a total of four chemically non-equivalent *ortho*- (**c** and **g**) and *meta*- (**b** and **f**) aromatic protons. These signals appear at -25.6, -20.5, -0.8 and 15.6 ppm for *ortho*-H, and at 12.8, 13.5, 14.9 and 15.6 ppm for *meta*-H.

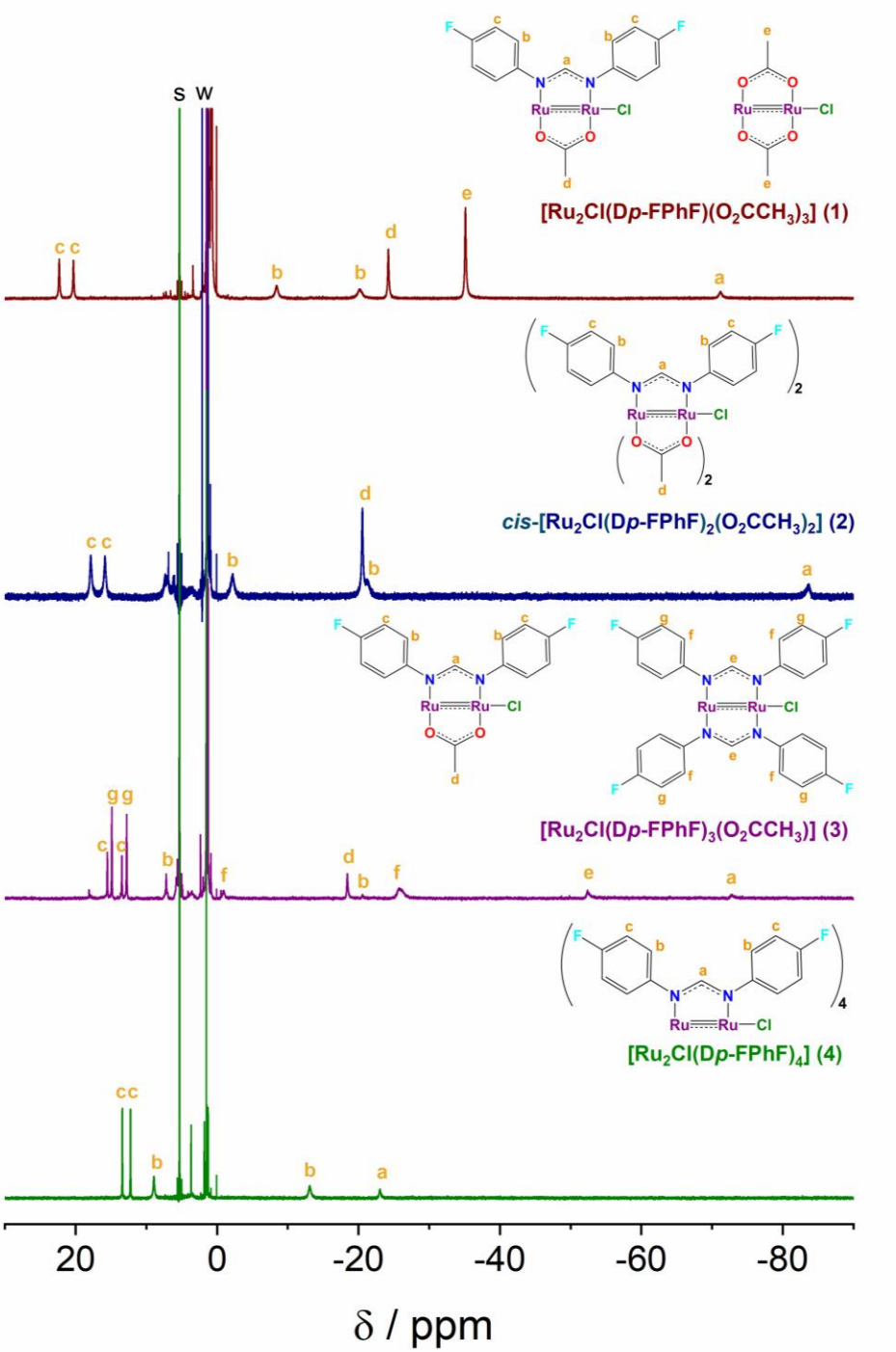

Fig. S38 Experimental low concentration ^{1}H-NMR spectra of compounds, from top to bottom, **1** (wine red), **2** (navy blue), **3** (purple) and **4** (olive green), measured in CD_2Cl_2 at 25 °C. The signal corresponding to the solvent is indicated with "s", while "w" is for water.

Table S10 ^{1}H-NMR experimental chemical shifts (ppm) of compounds **1**-**4**, measured in a low concentration CD_2Cl_2 at 25 °C. Number of protons assigned for each signal are given in parentheses.

Compound	-CH_3 (acetate)	-CH	*o*-C_{arom}-H	*m*-C_{arom}-H
1	-35.1(6H) -24.2(3H)	-71.1(1H)	-20.2(2H) -8.5(2H)	20.3(2H) 22.3(2H)
2	-20.5(6H)	-83.7(2H)	-21.2(4H) -2.2(4H)	15.8(4H) 17.8(4H)
3	-18.4(3H)	-72.7(1H) -52.4(2H)	-25.9(4H) -20.5(2H) -0.8(4H) 7.2(2H)	12.8(4H) 13.5(2H) 14.9(4H) 15.5(2H)
4	-	-23.0(4H)	-13.1(4H) 9.0(4H)	12.2(4H) 13.4(4H)

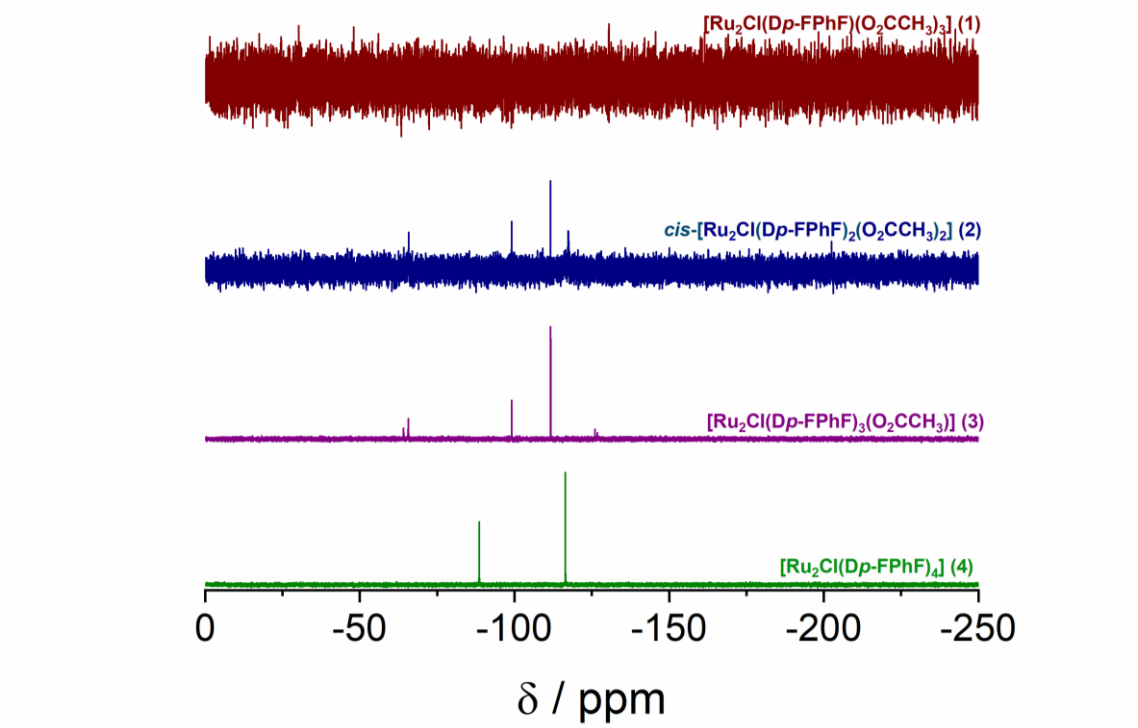

Fig. S39 Experimental high concentration ^{19}F-NMR spectra of compounds, from top to bottom, **1** (wine red), **2** (navy blue), **3** (purple) and **4** (olive green), measured in CD_2Cl_2 at 25 °C.

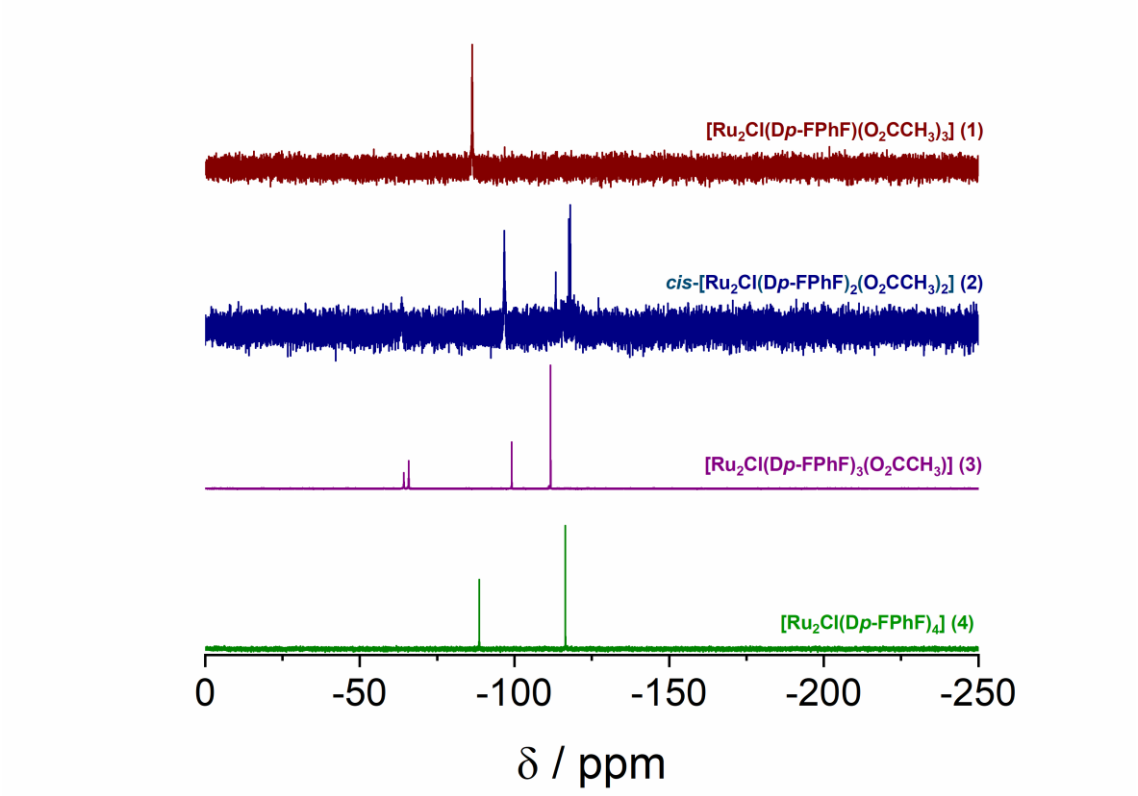

Fig. S40 Experimental low concentration ^{19}F-NMR spectra of compounds, from top to bottom, **1** (wine red), **2** (navy blue), **3** (purple) and **4** (olive green), measured in CD_2Cl_2 at 25 ^{o}C.

BIBLIOGRAPHY

1 R. W. Mitchell, A. Spencer and G. Wilkinson, *J. Chem. Soc., Dalton Trans.*, 1973, 846–854.

2 R. M. Roberts, *J. Org. Chem.*, 1949, **14**, 277–284.

3 P. Angaridis, F. A. Cotton, C. A. Murillo, D. Villagrán and X. Wang, *Inorg. Chem.*, 2004, **43**, 8290–8300.

4 T. Ikeue, Y. Kimura, K. Karino, M. Iida, T. Yamaji, I. Hiromitsu, T. Sugimori, D. Yoshioka, M. Mikuriya and M. Handa, *Inorg. Chem. Commun.*, 2013, **33**, 133–137.

5 W. R. Osterloh, G. Galindo, M. J. Yates, E. Van Caemelbecke and K. M. Kadish, *Inorg. Chem.*, 2020, **59**, 584–594.

6 T. A. Stephenson and G. Wilkinson, *J. Inorg. Nucl. Chem.*, 1966, **28**, 2285–2291.

7 M. W. Cooke, T. S. Cameron, K. N. Robertson, J. C. Swarts and M. A. S. Aquino, *Organometallics*, 2002, **21**, 5962–5971.

8 K. Nakamoto, in *Infrared and Raman Spectra of Inorganic and Coordination Compounds*, John Wiley & Sons, Ltd, Hoboken, New Jersey, 2009, vol. Part B, pp. 1–273.

9 F. D. Cukiernik, D. Luneau, J.-C. Marchon and P. Maldivi, *Inorg. Chem.*, 1998, **37**, 3698–3704.

10 J. Telser and R. S. Drago, *Inorg. Chem.*, 1984, **23**, 3114–3120.

11 J. Telser and R. S. Drago, *Inorg. Chem.*, 1985, **24**, 4765–4765.

12 Y. Harada, T. Ikeue, Y. Ide, Y. Kimura, I. Hiromitsu, D. Yoshioka, M. Mikuriya, Y. Kataoka and M. Handa, *Inorg. Chim. Acta*, 2015, **424**, 186–193.